Chapter 4

Development of sulfonamide based BChE inhibitors as anti-Alzheimer's agents through machine learning

4. Development of sulfonamide based BChE inhibitors as anti-Alzheimer's agents through machine learning

4.1. Introduction

Sulfonamides are the important chemical class of compounds that display versatile biological activity. In our previous studies, we explored various sulfonamide derivatives for the treatment of AD. The *piperazinedione sulfonamide* derivatives identified, through pharmacophore modelling and data mining, showed good inhibition profiles against AChE and BChE [147]. Further, *biphenyl sulfonamide* derivatives were synthesised and evaluated for inhibition against AChE, BChE and MMP [150]. These compounds were effective against scopolamine-induced amnesia in mice and amyloid β induced dementia in rats with a good pharmacological profile.

BChE is an exciting therapeutic target for AD, as the traditional ChE inhibitors have cholinergic side effects. The application of ML, especially ensemble learning, in identifying enzyme inhibitors has gained favour due to its high accuracy and low error rate [183-185]. In the present study, we investigated sulfonamides for BChE inhibition in the light of our earlier studies. A ML-based gradient boosting model was developed by using a set of BChE inhibitors. A sulfonamide library obtained from ZINC15 database was screened to identify *N-phenyl-4-(phenylsulfonamido) benzamide* as an active BChE inhibitor. Hence, a series of substituted *N-phenyl-4-(phenylsulfonamido) benzamides* were synthesised and characterised. The compounds were tested for AChE and BChE inhibition and cytotoxicity against SH-SY5Y. QSAR, molecular docking and MD study were performed to identify important features and binding patterns of the active compounds to the BChE enzyme. The compounds displaying good inhibition on BChE were further tested on scopolamine-induced amnesia in rats.

4.2. Materials and methods

4.2.1. Development of machine learning models for prediction of BChE inhibitors

BChE inhibitors were obtained from the ChEMBL database for the development of ML models [186]. Compounds with missing IC_{50} values, duplication and that were impermeable to BBB were removed. The SMILES strings of the compounds were deployed for PyBioMed descriptors and Daylight, Morgan, Molecular access system (MACCS) and ECFP4 fingerprints calculation using a python library (https://github.com/gadsbyfly/PyBioMed/) resulting in four datasets [187]. The descriptor sets were normalised for some of the multi-classification algorithms, while for others, no pre-processing was carried out. Further, a correlation filter (criterion: > 0.7) was applied to reduce features that showed a high degree of correlation. The IC_{50} values were converted to three classes with the labels 1 (most actives, $IC_{50} \leq 100$ nM), 2 (active, 100 nM > $IC_{50} \leq 1000$ nM) and 3 (moderately active, $IC_{50} > 1000$ nM). Fifteen algorithms, i.e., Logistic regression (LR), SVM, KNN, Ridge classifier, Perceptron, Linear discriminant analysis (LDA), Quadratic discriminant analysis (QDA), Label propagation, Label spreading, Primary aggressive classifier (PAC), decision tree, ensemble methods, viz., RF, gradient boosting and adaboost classifiers were implemented through scikit-learn ver. 0.24. The datasets were divided into four subsets, i.e., training, validation, and test sets (1 and 2). The training of the ML model was performed by using a training dataset with 5-fold cross-validation and was evaluated by using accuracy. Further, hyperparameter tuning was performed for each multiclass classification algorithm. The models displaying accuracy of at least 85 % or higher, on both training and validation sets, were selected. Finally, the selected models were evaluated on two independent test sets and final model was selected after comparing accuracy, precision, recall, and F1-score. The selected model was employed for the prediction of the virtual hits from the ZINC15 database that satisfied the applicability domain criteria.

4.2.2. Chemistry

The analytical grade reagents and solvents were used in the study. Pre-coated plates of silica gel 60 F254 (Merck KGaA) were used to monitor the progress of the reactions by thin-layer chromatography (TLC). Visualisation was carried out under ultraviolet light (254 nm) or in the presence of iodine vapours. The compounds were purified using column chromatography (silica gel, mesh size: 60-120) and their melting points were determined on automated melting point apparatus (Bamstead Electrothermal, UK). ATR spectra were recorded on Bruker Alpha_T(Germany) apparatus. The ^{1}H and ^{13}C NMR spectra were recorded in d^{6}-DMSO on the Bruker 500 FT-NMR spectrometer with the operating frequency of 500 MHz and 125 MHz, respectively. The chemical shift was calculated in ppm (δ), and the coupling constant (*J*) was measured in Hz. Mass spectra were acquired with a UPLC/XEVO G2-XS QTOF instrument equipped with APCI and ESI multimode ionisation source. The purity of the compounds was determined by Agilent 1260 Infinity II Quaternary LC (a quaternary pump with a DAD HS G7115A detector, l ¼ 315 nm). The isocratic mobile phase was delivered by quaternary pumps with a flow rate of 1 ml/min. The mobile phase composition was phase A (acetonitrile) and phase B (methanol) in the ratio of 9:1. 20 μL samples were injected into the HPLC column (Agilent ZORBAX Eclipse plus C8 column, dimensions: 5 μm, 4.6 × 250 mm). The compounds were detected at 315 nm wavelength. The purity of the compounds was found to be more than 98%.

4.2.2.1. General procedure for the synthesis of *4-(phenylsulfonamido) benzoic acid* (3)

A mixture of 30 mL water and 10 mL acetone was used to dissolve *para*-aminobenzoic acid (PABA) (0.0073 moles, one equivalent) and sodium carbonate (0.0219 mol, three equivalent). *Benzene sulfonyl chloride* (0.0073 mol, one equivalent) in 20 mL of acetone was added to the reaction mixture and stirred at room temperature (RT) for 24 hrs. The

progress of the reaction was monitored by TLC using ethyl acetate and hexane (4:6) as the mobile phase. Acetone was evaporated under reduced pressure on the completion of the reaction. It was followed by neutralisation with 1 N HCl to obtain the crude product. The product was filtered and recrystallised using 20 % ethanol [147, 188].

***4-(phenylsulfonamido) benzoic acid* (3)**

Crimson white solid (1.878 g, 89.9 % yield). M.P.: 175 – 181 ºC, R_f = 0.23 (EA/Hex, 4:6, v/v). IR (ATR): 3271 (secondary NH stretching), 1678 (C=O stretching), 1336 (asymm. S=O stretching) and 1182 (symm. S=O stretching) cm^{-1}. ^1H NMR (500 MHz, DMSO-d6): δ = 12.75 (s, 1H, COOH), 10.83 (s, 1H, SO_2NH), 7.73 – 7.79 (m, 4H, Ar-H), 7.65 – 7.62 (m, 1H, Ar-H), 7.59 – 7.56 (t, *J* = 7.5 Hz, 2H, Ar-H), 7.21 – 7.19 (d, *J* = 8.8 Hz, 2H, Ar-H). ^{13}C NMR (125 MHz, DMSO-d6): δ = 164.98, 143.18, 141.80, 139.70, 135.96, 134.95, 133.72, 129.92, 129.57, 129.48, 128.98, 127.16, 126.32, 125.27, 118.83, 20.51. MS (EI+): *m/z* calculated for $C_{13}H_{11}NO_4S$ 277.29, found – 277.36 (M^+).

4.2.2.2. General procedure for the synthesis of substituted *N-phenyl-4-(phenyl sulfonamido) benzamide* derivatives (30-55)

Compound **3** (0.0009 moles, 1 equivalent) and *triethylamine* (0.0027 mole, 3 equivalent) were dissolved in 25 mL of DCM. Substituted *anilines* (**4 - 29**) or aliphatic *amines* (**63 – 69**) (1.1 equivalent) were added to the reaction mixture, followed by dropwise addition of an excess of *thionyl chloride* (0.00045, 5 equivalent). The reaction was continuously stirred for 6-8 hrs, followed by evaporation of DCM under reduced pressure. The obtained residue was washed with a saturated sodium bicarbonate solution and extracted with ethyl acetate. The product was purified with column chromatography using ethyl acetate in hexane over silica gel (60-120 mesh).

***N-phenyl-4-(phenylsulfonamido) benzamide* (30)**

Brown solid (0.191 g, 60.12 % yield). M.P.: 171 – 174˚C, R_f = 0.34 (EA/Hex, 4:6, v/v). IR (ATR): 3258 (secondary NH stretching), 1647 (C=O stretching), 1325 (asymm. S=O stretching) and 1155 (symm. S=O stretching) cm^{-1}. ^1H NMR (500 MHz, DMSO-d6): δ = 10.76 (s, 1H, SO_2NH), 10.09 (s, 1H, CONH), 7.86 – 7.80 (m, 4H, Ar-H), 7.72 – 7.70 (d, *J* = 7.8 Hz, 2H, Ar-H), 7.66 – 7.62 (m, 1H, Ar-H), 7.60 – 7.57 (t, *J* = 7.5 Hz, 2H, Ar-H), 7.34 – 7.31 (m, 2H, Ar-H), 7.23 – 7.22 (d, *J* = 8.7 Hz, 2H, Ar-H), 7.09 – 7.06 (t, *J* = 6.9 Hz, 1H, Ar-H). ^{13}C NMR (125 MHz, DMSO-d6): δ = 165.27, 141.25, 139.81, 139.61, 133.64, 130.45, 129.89, 129.46, 129.03, 127.16, 124.01, 120.73, 118.80. MS (EI+): *m/z* calculated for $C_{19}H_{16}N_2O_3S$ 352.41, found – 352.33 (M^+).

***N-(2-fluorophenyl)-4-(phenylsulfonamido) benzamide* (31)**

Brown solid (0.248 g, 74.27 % yield). M.P.: 159 – 163˚C, R_f = 0.47 (EA/Hex, 4:6, v/v). IR (ATR): 3212 (secondary NH stretching), 1645 (C=O stretching), 1314 (asymm. S=O stretching) and 1156 (symm. S=O stretching) cm^{-1}. ^1H NMR (500 MHz, DMSO-d6): δ = 10.79 (s, 1H, SO_2NH), 9.97 (s, 1H, CONH), 7.86 – 7.84 (m, 4H, Ar-H), 7.66 – 7.53 (m, 4H, Ar-H), 7.30 – 7.15 (m, 5H, Ar-H). ^{13}C NMR (125 MHz, DMSO-d6): δ = 169.86, 161.95, 159.99, 146.25, 144.50, 138.42, 134.64, 134.37, 134.13, 132.30, 131.91, 131.00, 130.90, 129.48, 123.58, 123.51, 121.08, 120.92. MS (EI+): *m/z* calculated for $C_{19}H_{15}FN_2O_3S$ 370.40, found – 371.37 (M^+).

***N-(3-fluorophenyl)-4-(phenylsulfonamido) benzamide* (32)**

White solid (0.15 g, 44.92 % yield). M.P.: 177 -– 181˚C, R_f = 0.38 (EA/Hex, 4:6, v/v). IR (ATR): 3259 (secondary NH stretching), 1649 (C=O stretching), 1336 (asymm. S=O stretching) and 1159 (symm. S=O stretching) cm^{-1}. ^1H NMR (500 MHz, DMSO-d6): δ = 10.79 (s, 1H, SO_2NH), 10.28 (s, 1H, CONH), 7.86 – 7.82 (m, 4H, Ar-H), 7.71 – 7.69 (d, *J* = 11.7 Hz, 1H, Ar-H), 7.66 – 7.63 (m, 1H, Ar-H), 7.60 – 7.57 (t, *J* = 7.4 Hz, 2H, Ar-H),

7.51 – 7.50 (d, *J* = 8.2 Hz, 1H, Ar-H), 7.38 – 7.34 (dd, *J* = 15.3, 7.7 Hz, 1H, Ar-H), 7.25 – 7.23 (d, *J* = 8.1 Hz, 2H, Ar-H), 6.92 – 6.89 (t, *J* = 8.3 Hz, 1H, Ar-H). ^{13}C NMR (125 MHz, DMSO-d6): δ = 165.55, 163.46, 161.54, 141.44, 139.76, 133.67, 130.69, 130.62, 130.09, 129.90, 129.57, 127.18, 118.77, 116.31, 110.51, 110.34, 107.40, 107.19. MS (EI+): *m/z* calculated for $C_{19}H_{15}FN_2O_3S$ 370.40, found – 371.45 (M^+).

N-(4-fluorophenyl)-4-(phenylsulfonamido) benzamide **(33)**

buff yellow solid (0.175 g, 52.41 % yield). M.P.: 174 –178˚C, R_f = 0.38 (EA/Hex, 4:6, v/v). IR (ATR): 3259 (secondary NH stretching), 1649 (C=O stretching), 1340 (asymm. S=O stretching) and 1158 (symm. S=O stretching) cm^{-1}. ^{1}H NMR (500 MHz, DMSO-d6): δ = 10.77 (s, 1H, SO_2NH), 10.15 (s, 1H, CONH), 7.84 – 7.80 (m, 4H, Ar-H), 7.74 – 7.71 (dd, *J* = 9.2, 5.1 Hz, 2H, Ar-H), 7.64 – 7.61 (m, 1H, Ar-H), 7.59 – 7.57 (t, *J* = 7.4 Hz, 2H, Ar-H), 7.24 – 7.21 (t, *J* = 7.3 Hz, 2H, Ar-H), 7.18 – 7.15 (t, *J* = 8.9 Hz, 2H, Ar-H). ^{13}C NMR (125 MHz, DMSO-d6): δ = 165.18, 141.26, 139.76, 133.66, 130.29, 129.90, 129.46, 127.17, 122.54, 122.48, 118.79, 115.70, 115.53. MS (EI+): *m/z* calculated for $C_{19}H_{15}FN_2O_3S$ 370.40, found – 371.48 (M^+).

N-(2-chlorophenyl)-4-(phenylsulfonamido) benzamide **(34)**

Crimson white solid (0.24 g, 68.82 % yield). M.P.: 145 –148˚C, R_f = 0.5 (EA/Hex, 4:6, v/v). IR (ATR): 3233 (secondary NH stretching), 1678 (C=O stretching), 1308 (asymm. S=O stretching) and 1156 (symm. S=O stretching) cm^{-1}. ^{1}H NMR (500 MHz, DMSO-d6): δ = 10.79 (s, 1H, SO_2NH), 9.91 (s, 1H, CONH), 7.87 – 7.84 (t, *J* = 8.0 Hz, 4H, Ar-H), 7.63 – 7.62 (t, *J* = 7.2 Hz, 1H, Ar-H), 7.59 – 7.52 (m, 4H, Ar-H), 7.37 – 7.34 (t, *J* = 7.6 Hz, 1H, Ar-H), 7.28 – 7.23 (m, 3H, Ar-H). ^{13}C NMR (125 MHz, DMSO-d6): δ = 165.09, 141.50, 133.68, 129.98, 129.91, 129.54, 129.40, 12 8.81, 127.91, 127.85, 127.17, 118.83. MS (EI+): *m/z* calculated for $C_{19}H_{15}ClN_2O_3S$ 386.85, found – 387.05, 389.05 [M^+, M^{+2} (3:1)].

***N-(3-chlorophenyl)-4-(phenylsulfonamido) benzamide* (35)**

Crimson white solid (0.21 g, 60.22 % yield). M.P.: 178 – 183˚C, R_f = 0.44 (EA/Hex, 4:6, v/v). IR (ATR): 3367 (secondary NH stretching), 1678 (C=O stretching), 1308 (asymm. S=O stretching) and 1156 (symm. S=O stretching) cm^{-1}. ^1H NMR (500 MHz, DMSO-d6): δ = 10.80 (s, 1H, SO_2NH), 10.25 (s, 1H, CONH), 7.91 (s, 1H, Ar-H), 7.85-7.81 (m, 4H, Ar-H), 7.65 – 7.62 (t, *J* = 7.0 Hz, 2H, Ar-H), 7.60 – 7.57 (t, *J* = 7.5 Hz, 2H, Ar-H), 7.37 – 7.34 (t, *J* = 8.1 Hz, 1H, Ar-H), 7.25 – 7.23 (d, *J* = 8.6 Hz, 2H, Ar-H), 7.14 – 7.13 (d, *J* = 7.8 Hz, 1H, Ar-H). ^{13}C NMR (125 MHz, DMSO-d6): δ = 165.53, 141.46, 141.13, 139.75, 133.68, 133.37, 130.75, 130.00, 129.91, 129.58, 127.17, 123.68, 120.05, 118.98, 118.76. MS (EI+): *m/z* calculated for $C_{19}H_{15}ClN_2O_3S$ 386.85, found – 387.07, 389.07 [M^+, M^{+2} (3:1)].

***N-(4-chlorophenyl)-4-(phenylsulfonamido) benzamide* (36)**

White solid (0.189 g, 54.19 % yield). M.P.: 181 –185˚C, R_f = 0.38 (EA/Hex, 4:6, v/v). IR (ATR): 3255 (secondary NH stretching), 1649 (C=O stretching), 1338 (asymm. S=O stretching) and 1163 (symm. S=O stretching) cm^{-1}. ^1H NMR (500 MHz, DMSO-d6): δ = 10.77 (s, 1H, SO_2NH), 10.21 (s, 1H, CONH), 7.85 – 7.81 (dd, *J* = 13.3, 8.1 Hz, 4H, Ar-H), 7.76 – 7.74 (d, *J* = 8.8 Hz, 2H, Ar-H), 7.65 – 7.62 (m, 1H, Ar-H), 7.59 – 7.56 (t, *J* = 7.5 Hz, 2H, Ar-H), 7.39 – 7.37 (d, *J* = 8.8 Hz, 2H, Ar-H), 7.24 – 7.22 (d, *J* = 8.6 Hz, 2H, Ar-H). ^{13}C NMR (125 MHz, DMSO-d6): δ = 165.37, 141.36, 139.76, 138.61, 133.67, 130.16, 129.90, 129.52, 128.95, 127.61, 127.17, 122.21, 118.78. MS (EI+): *m/z* calculated for $C_{19}H_{15}ClN_2O_3S$ 386.85, found – 387.2, 389.02 [M^+, M^{+2} 3:1)].

***N-(2-bromophenyl)-4-(phenylsulfonamido) benzamide* (37)**

Crimson white solid (0.22 g, 56.58 % yield). M.P.: 163 – 168˚C, R_f = 0.53 (EA/Hex, 4:6, v/v). IR (ATR): 3354 (secondary NH stretching), 1646 (C=O stretching), 1309 (asymm. S=O stretching) and 1152 (symm. S=O stretching) cm^{-1}. ^1H NMR (500 MHz, DMSO-

d6): δ = 10.80 (s, 1H, SO_2NH), 9.90 (s, 1H, CONH), 7.88 – 7.85 (m, 4H, Ar-H), 7.70 – 7.60 (m, 4H, Ar-H), 7.52 – 7.51 (d, *J* = 7.2 Hz, 1H, Ar-H), 7.42 – 7.39 (m, 1H, Ar-H), 7.25 – 7.21 (m, 3H, Ar-H). ^{13}C NMR (125 MHz, DMSO-d6): δ = 165.03, 141.49, 139.74, 136.96, 133.69, 133.10, 129.92, 129.51, 129.26, 128.54, 128.34, 127.17, 121.00, 118.82. MS (EI+): *m/z* calculated for $C_{19}H_{15}BrN_2O_3S$ 431.30, found – 431.01, 433.0 [M^+, M^{+2} (1:1)].

***N-(3-bromophenyl)-4-(phenylsulfonamido) benzamide* (38)**

0.269 g of compound **38** as a crimson white solid (69.18 % yield). M.P.: 174 –178˚C, R_f = 0.4 (EA/Hex, 4:6, v/v). IR (ATR): 3362 (secondary NH stretching), 1649 (C=O stretching), 1313 (asymm. S=O stretching) and 1155 (symm. S=O stretching) cm^{-1}. ^{1}H NMR (500 MHz, DMSO-d6): δ = 10.79 (s, 1H, SO_2NH), 10.24 (s, 1H, CONH), 8.06 (s, 1H, Ar-H), 7.86 – 7.82 (m, 4H, Ar-H), 7.71 – 7.69 (d, *J* = 7.7 Hz, 1H, Ar-H), 7.66 – 7.63 (m, 1H, Ar-H), 7.60 – 7.57 (t, *J* = 7.5 Hz, 2H, Ar-H), 7.32 – 7.23 (m, 4H, Ar-H). ^{13}C NMR (125 MHz, DMSO-d6): δ = 165.48, 141.47, 141.29, 139.77, 133.67, 131.05, 130.00, 129.90, 129.58, 127.18, 126.56, 122.91, 121.84, 119.36, 118.76. MS (EI+): *m/z* calculated for $C_{19}H_{15}BrN_2O_3S$ 431.30, found – 431.03, 433.01 [M^+, M^{+2} (1:1)].

***N-(4-bromophenyl)-4-(phenylsulfonamido) benzamide* (39)**

Crimson white solid (0.25 g, 64.3 % yield). M.P.: 216 – 219˚C, R_f = 0.4 (EA/Hex, 4:6, v/v). IR (ATR): 3257 (secondary NH stretching), 1650 (C=O stretching), 1332 (asymm. S=O stretching) and 1163 (symm. S=O stretching) cm^{-1}. ^{1}H NMR (500 MHz, DMSO-d6): δ = 10.77 (s, 1H, SO_2NH), 10.21 (s, 1H, CONH), 7.85 – 7.51 (m, 4H, Ar-H), 7.71 – 7.69 (d, *J* = 8.8 Hz, 2H, Ar-H), 7.65 – 7.62 (t, *J* = 7.2 Hz, 1H, Ar-H), 7.59 – 7.56 (t, *J* = 7.5 Hz, 2H, Ar-H), 7.52 – 7.50 (d, *J* = 8.7 Hz, 2H, Ar-H), 7.24 – 7.22 (d, *J* = 8.5 Hz, 2H, Ar-H). ^{13}C NMR (125 MHz, DMSO-d6): δ = 165.37, 141.37, 139.76, 139.04, 133.67,

131.87, 130.16, 129.90, 129.54, 127.17, 122.56, 118.77, 115.66. MS (EI+): *m/z* calculated for $C_{19}H_{15}BrN_2O_3S$ 431.30, found – 431, 433.1 [M^+, M^{+2} (1:1)].

***N-(2-methoxyphenyl)-4-(phenylsulfonamido) benzamide* (40)**

Pearl coloured solid (0.192 g, 55.69 % yield). M.P.: 140 – 144˚C, R_f = 0.34 (EA/Hex, 4:6, v/v). IR (ATR): 3207 (secondary NH stretching), 1646 (C=O stretching), 1339 (asymm. S=O stretching) and 1155 (symm. S=O stretching) cm^{-1}. ^1H NMR (500 MHz, DMSO-d6): δ = 10.76 (s, 1H, SO_2NH), 9.29 (s, 1H, CONH), 7.85 – 7.83 (m, 4H, Ar-H), 7.72 – 7.70 (dd, *J* = 7.8, 1.1 Hz, 1H, Ar-H), 7.65 – 7.32 (t, *J* = 7.3 Hz, 1H, Ar-H), 7.60 – 7.57 (t, *J* = 7.5 Hz, 2H, Ar-H), 7.23 – 7.21 (d, *J* = 8.7 Hz, 2H, Ar-H), 7.17 – 7.14 (m, 1H, Ar-H), 7.07 – 7.06 (d, *J* = 7.6 Hz, 1H, Ar-H), 6.96 – 6.93 (t, *J* = 7.6 Hz, 1H, Ar-H), 3.80 (s, 3H, OCH_3). ^{13}C NMR (125 MHz, DMSO-d6): δ = 164.65, 151.89, 141.28, 139.78, 133.66, 129.96, 129.90, 129.31, 127.27, 127.15, 126.09, 124.70, 120.63, 118.86, 111.80, 56.12. MS (EI+): *m/z* calculated for $C_{20}H_{18}N_2O_4S$ 382.43, found – 382.40 (M^+).

***N-(4-methoxyphenyl)-4-(phenylsulfonamido) benzamide* (41)**

Pearl coloured solid (0.264 g, 76.57 % yield). M.P.: 174 – 178˚C, R_f = 0.22 (EA/Hex, 4:6, v/v). IR (ATR): 3269 (secondary NH stretching), 1646 (C=O stretching), 1334 (asymm. S=O stretching) and 1158 (symm. S=O stretching) cm^{-1}. ^1H NMR (500 MHz, DMSO-d6): δ = 10.74 (s, 1H, SO_2NH), 9.97 (s, 1H, CONH), 7.85 – 7.81 (m, 4H, Ar-H), 7.64 – 7.57 (dt, *J* = 14.9, 6.3 Hz, 5H, Ar-H), 7.23 – 7.21 (d, *J* = 8.5 Hz, 2H, Ar-H), 6.91 – 6.89 (d, *J* = 8.9 Hz, 2H, Ar-H), 3.73 (s, 3H, OCH_3). ^{13}C NMR (125 MHz, DMSO-d6): δ = 164.83, 155.94, 141.04, 139.80, 133.63, 132.69, 130.61, 129.88, 129.33, 127.17, 122.35, 118.85, 114.17, 55.62. MS (EI+): *m/z* calculated for $C_{20}H_{18}N_2O_4S$ 382.43, found – 382.37 (M^+).

***N-(2-nitrophenyl)-4-(phenylsulfonamido) benzamide* (42)**

Yellow solid (0.132 g, 36.85 % yield). M.P.: 164 – 167˚C, R_f = 0.53 (EA/Hex, 4:6, v/v). IR (ATR): 3284 (secondary NH stretching), 1667 (C=O stretching), 1338 (asymm. S=O stretching) and 1156 (symm. S=O stretching) cm^{-1}. ^1H NMR (500 MHz, DMSO-d6): δ = 10.84 (s, 1H, SO_2NH), 10.62 (s, 1H, CONH), 7.99 – 7.98 (d, *J* = 7.9 Hz, 1H, Ar-H), 7.86 – 7.82 (m, 4H, Ar-H), 7.73 – 7.71 (m, 2H, Ar-H), 7.66 – 7.62 (m, 1H, Ar-H), 7.60 – 7.57 (m, 2H, Ar-H), 7.42 – 7.38 (ddd, *J* = 8.5, 5.3, 3.5 Hz, 1H, Ar-H), 7.27-7.25 (d, *J* = 8.7 Hz, 2H, Ar-H). ^{13}C NMR (125 MHz, DMSO-d6): δ = 165.05, 143.27, 141.91, 139.70, 134.44, 133.73, 132.02, 129.93, 129.65, 128.87, 127.17, 126.24, 125.90, 125.40, 118.82. MS (EI+): *m/z* calculated for $C_{19}H_{15}N_3O_5S$ 397.41, found – 397.40 (M^+).

***N-(3-nitrophenyl)-4-(phenylsulfonamido) benzamide* (43)**

Brownish yellow solid (0.225 g, 62.8 % yield). M.P.: 185 – 189˚C, R_f = 0.31 (EA/Hex, 4:6, v/v). IR (ATR): 3148 (secondary NH stretching), 1649 (C=O stretching), 1297 (asymm. S=O stretching) and 1153 (symm. S=O stretching) cm^{-1}. ^1H NMR (500 MHz, DMSO-d6): δ = 10.83 (s, 1H, SO_2NH), 10.55 (s, 1H, CONH), 8.75 – 8.74 (t, *J* = 2.2 Hz, 1H, Ar-H), 8.14 – 8.12 (m, 1H, Ar-H), 7.94 – 7.93 (ddd, *J* = 8.2, 2.3, 0.9 Hz, 1H, Ar-H), 7.87 – 7.84 (m, 4H, Ar-H), 7.65 – 7.57 (m, 4H, Ar-H), 7.26 – 7.24 (d, *J* = 8.8 Hz, 2H, Ar-H). ^{13}C NMR (125 MHz, DMSO-d6): δ = 165.75, 148.35, 141.67, 140.86, 139.74, 133.70, 130.50, 129.92, 129.68, 129.62, 127.18, 126.52, 118.72, 118.47, 114.67. MS (EI+): *m/z* calculated for $C_{19}H_{15}N_3O_5S$ 397.41, found – 397.46 (M^+).

***N-(4-nitrophenyl)-4-(phenylsulfonamido) benzamide* (44)**

Yellow solid (0.26 g, 72.57 % yield). M.P.: 166 – 170˚C, R_f = 0.31 (EA/Hex, 4:6, v/v). IR (ATR): 3247 (secondary NH stretching), 1651 (C=O stretching), 1333 (asymm. S=O stretching) and 1158 (symm. S=O stretching) cm^{-1}. ^1H NMR (500 MHz, DMSO-d6): δ = 10.85 (s, 1H, SO_2NH), 10.66 (s, 1H, CONH), 8.25 – 8.23 (d, *J* = 9.2 Hz, 2H, Ar-H), 8.01

– 7.99 (d, *J* = 9.2 Hz, 2H, Ar-H), 7.86 – 7.85 (d, *J* = 8.4 Hz, 4H, Ar-H), 7.66 – 7.57 (t, *J* = 7.3 Hz, 1H, Ar-H), 7.60 – 7.57 (t, *J* = 7.5 Hz, 2H, Ar-H), 7.26 – 7.24 (d, *J* = 8.7 Hz, 2H, Ar-H). ^{13}C NMR (125 MHz, DMSO-d6): δ = 165.97, 146.00, 142.81, 141.81, 139.73, 133.71, 129.93, 129.87, 129.57, 127.18, 125.26, 120.15, 118.66. MS (EI+): *m/z* calculated for $C_{19}H_{15}N_3O_5S$ 397.41, found – 397.47 (M^+).

***4-(phenylsulfonamido)-N-(2-(trifluoromethyl)phenyl) benzamide* (45)**

Cream solid (0.183 g, 48.29 % yield). M.P.: 171 –174˚C, R_f = 0.46 (EA/Hex, 4:6, v/v). IR (ATR): 3267 (secondary NH stretching), 1659 (C=O stretching), 1318 (asymm. S=O stretching) and 1154 (symm. S=O stretching) cm^{-1}. ^{1}H NMR (500 MHz, DMSO-d6): δ = 10.79 (s, 1H, SO_2NH), 9.99 (s, 1H, CONH), 7.86 – 7.82 (m, 4H, Ar-H), 7.78 – 7.77 (d, *J* = 7.8 Hz, 1H, Ar-H), 7.73 – 7.70 (t, *J* = 7.5 Hz, 1H, Ar-H), 7.66 – 7.63 (t, *J* = 7.3 Hz, 1H, Ar-H), 7.60 – 7.57 (t, *J* = 7.4 Hz, 2H, Ar-H), 7.53 – 7.48 (dd, *J* = 17.8, 7.9 Hz, 2H, Ar-H), 7.25 – 7.24 (d, *J* = 8.8 Hz, 2H, Ar-H). ^{13}C NMR (125 MHz, DMSO-d6): δ = 166.02, 141.51, 139.80, 136.27, 133.66, 133.52, 131.68, 129.90, 129.46, 129.34, 127.83, 127.17, 126.93, 126.88, 126.70, 125.16, 122.99, 118.81, 60.22. MS (EI+): *m/z* calculated for $C_{20}H_{15}F_3N_2O_3S$ 420.41, found – 420.43 (M^+).

***4-(phenylsulfonamido)-N-(3-(trifluoromethyl)phenyl) benzamide* (46)**

Cream solid (0.224 g, 59.1 % yield). M.P.: 191 – 195˚C, R_f = 0.44 (EA/Hex, 4:6, v/v). IR (ATR): 3367 (secondary NH stretching), 1656 (C=O stretching), 1327 (asymm. S=O stretching) and 1154 (symm. S=O stretching) cm^{-1}. ^{1}H NMR (500 MHz, DMSO-d6): δ = 10.81 (s, 1H, SO_2NH), 10.40 (s, 1H, CONH), 8.19 (s, 1H, Ar-H), 7.99 – 7.98 (d, *J* = 8.3 Hz, 1H, Ar-H), 7.85 – 7.84 (d, *J* = 8.7 Hz, 4H, Ar-H), 7.66 – 7.63 (t, *J* = 7.3 Hz, 1H, Ar-H), 7.60 – 7.56 (m, 3H, Ar-H), 7.44 – 7.42 (d, *J* = 7.7 Hz, 1H, Ar-H), 7.25 – 7.23 (d, *J* = 8.7 Hz, 2H, Ar-H). ^{13}C NMR (125 MHz, DMSO-d6): δ = 165.65, 141.55, 140.44, 139.74,

133.69, 130.31, 129.91, 129.86, 129.61, 127.18, 124.11, 118.74, 116.68. MS (EI+): *m/z* calculated for $C_{20}H_{15}F_3N_2O_3S$ 420.41, found – 420.46 (M^+).

***N-(3-acetylphenyl)-4-(phenylsulfonamido) benzamide* (47)**

Light brown solid (0.145 g, 40.78 % yield). M.P.:146 –149˚C, R_f = 0.26 (EA/Hex, 4:6, v/v). IR (ATR): 3354 (secondary NH stretching), 1680 (C=O stretching), 1311 (asymm. S=O stretching) and 1151 (symm. S=O stretching) cm^{-1}. ^1H NMR (500 MHz, DMSO-d6): δ = 10.79 (s, 1H, SO_2NH), 10.29 (s, 1H, CONH), 8.31 (t, *J* = 1.8 Hz, 1H, Ar-H), 8.02 – 8.00 (m, 1H, Ar-H), 7.86 – 7.84 (m, 4H, Ar-H), 7.70 – 7.68 (m, 1H, Ar-H), 7.64 – 7.62 (dd, *J* = 5.0, 3.7 Hz, 1H, Ar-H), 7.60 – 7.57 (m, 2H, Ar-H), 7.50 – 7.47 (t, *J* = 7.9 Hz, 1H, Ar-H), 7.24 – 7.23 (d, *J* = 8.8 Hz, 2H, Ar-H), 2.57 (s, 3H, CH_3). ^{13}C NMR (125 MHz, DMSO-d6): δ = 198.13, 165.43, 141.42, 140.04, 139.77, 137.67, 133.68, 130.06, 129.91, 129.55, 129.49, 127.17, 125.14, 124.00, 120.00, 118.75, 27.22. MS (EI+): *m/z* calculated for $C_{21}H_{18}N_2O_4S$ 394.45, found – 394.47 (M^+).

***N-(4-acetylphenyl)-4-(phenylsulfonamido) benzamide* (48)**

Light brown solid (0.12 g. 33.75 % yield). M.P.: 197 – 201˚C, R_f = 0.22 (EA/Hex, 4:6, v/v). IR (ATR): 3285 (secondary NH stretching), 1673 (C=O stretching), 1395 (asymm. S=O stretching) and 1158 (symm. S=O stretching) cm^{-1}. ^1H NMR (500 MHz, DMSO-d6): δ = 10.81 (s, 1H, SO_2NH), 10.40 (s, 1H, CONH), 7.96 – 7.94 (m, 2H, Ar-H), 7.89 – 7.87 (m, 2H, Ar-H), 7.85 – 7.83 (m, 4H, Ar-H), 7.66 – 7.62 (m, 1H, Ar-H), 7.60 – 7.57 (m, 2H, Ar-H), 7.25 – 7.23 (m, 2H, Ar-H), 2.54 (s, 3H, CH_3). ^{13}C NMR (125 MHz, DMSO-d6): δ = 198.13, 165.43, 141.42, 140.04, 139.77, 137.67, 133.68, 130.06, 129.91, 129.55, 129.49, 127.17, 125.14, 124.00, 120.00, 118.75, 27.22. MS (EI+): *m/z* calculated for $C_{21}H_{18}N_2O_4S$ 394.45, found – 394.44 (M^+).

***4-(phenylsulfonamido)-N-(o-tolyl) benzamide* (49)**

Brown yellow solid (0.16 g, 48.43 % yield). M.P. :163 – 167˚C, R_f = 0.44 (EA/Hex, 4:6, v/v). IR (ATR): 3278 (secondary NH stretching), 1647 (C=O stretching), 1337 (asymm. S=O stretching) and 1158 (symm. S=O stretching) cm^{-1}. ^1H NMR (500 MHz, DMSO-d6): δ = 10.74 (s, 1H, SO_2NH), 10.01 (s, 1H, CONH), 7.84 – 7.79 (m, 4H, Ar-H), 7.65 – 7.62 (ddd, *J* = 6.5, 3.8, 1.3 Hz, 1H, Ar-H), 7.59 – 7.56 (m, 4H, Ar-H), 7.23 – 7.20 (m, 2H, Ar-H), 7.13 – 7.12 (d, J = 8.3 Hz, 2H, Ar-H), 2.26 (s, 3H, CH_3). ^{13}C NMR (125 MHz, DMSO-d6): δ = 165.04, 141.09, 139.77, 137.09, 133.65, 132.94, 130.58, 129.89, 129.42, 129.40, 127.16, 120.74, 118.80, 20.94. MS (EI+): *m/z* calculated for $C_{20}H_{18}N_2O_3S$ 366.44, found – 366.49 (M^+).

***4-(phenylsulfonamido)-N-(m-tolyl) benzamide* (50)**

Brown yellow solid (0.13 g, 39.35 % yield). M.P. :176 –179˚C, R_f = 0.46 (EA/Hex, 4:6, v/v). IR (ATR): 3273 (secondary NH stretching), 1645 (C=O stretching), 1338 (asymm. S=O stretching) and 1159 (symm. S=O stretching) cm^{-1}. ^1H NMR (500 MHz, DMSO-d6): δ = 10.72 (s, 1H, SO_2NH), 9.97 (s, 1H, CONH), 7.81 – 7.76 (m, 4H, Ar-H), 7.62 – 7.59 (t, *J* = 7.3 Hz, 1H, Ar-H), 7.56 – 7.52 (dd, *J* = 14.3, 7.1 Hz, 3H, Ar-H), 7.47 – 7.45 (d, *J* = 8.1 Hz, 1H, Ar-H), 7.19 – 7.14 (m, 3H, Ar-H), 6.86 – 6.85 (d, *J* = 7.4 Hz, 1H, Ar-H), 2.25 (s, 3H, CH_3). ^{13}C NMR (125 MHz, DMSO-d6): δ = 169.92, 145.91, 144.53, 144.29, 142.90, 135.27, 134.65, 134.20, 131.92, 123.56, 26.42. MS (EI+): m/z calculated for $C_{20}H_{18}N_2O_3S$ 366.44, found – 366.46 (M^+).

***4-(phenylsulfonamido)-N-(p-tolyl) benzamide* (51)**

Buff yellow solid (0.2 g 60.54 % yield). M.P.: 172 – 177˚C, R_f = 0.38 (EA/Hex, 4:6, v/v). IR (ATR): 3278 (secondary NH stretching), 1649 (C=O stretching), 1336 (asymm. S=O stretching) and 1160 (symm. S=O stretching) cm^{-1}. ^1H NMR (500 MHz, DMSO-d6): δ = 10.74 (s, 1H, SO_2NH), 10.01 (s, 1H, CONH), 7.85 – 7.81 (dd, *J* = 13.3, 8.0 Hz, 4H, Ar-

H), 7.65 – 7.58 (m, 5H, Ar-H), 7.23 – 7.22 (d, *J* = 8.3 Hz, 2H. Ar-H), 7.14 – 7.12 (d, *J* = 8.0 Hz, 2H, Ar-H), 2.26 (s, 3H, CH_3). ^{13}C NMR (125 MHz, DMSO-d6): δ = 165.05, 141.11, 139.80, 137.10, 133.64, 132.94, 130.59, 129.88, 129.42, 127.17, 120.76, 118.82, 20.94. MS (EI+): *m/z* calculated for $C_{20}H_{18}N_2O_3S$ 366.44, found – 366.46 (M^+).

***N-(2,4-dimethylphenyl)-4-(phenylsulfonamido) benzamide* (52)**

Yellow brown solid (0.159 g, 46.36 % yield). M.P.: 183 –186˚C, R_f = 0.31 (EA/Hex, 4:6, v/v). IR (ATR): 3282 (secondary NH stretching), 1649 (C=O stretching), 1300 (asymm. S=O stretching) and 1152 (symm. S=O stretching) cm^{-1}. ^1H NMR (500 MHz, DMSO-d6): δ = 10.74 (s, 1H, SO_2NH), 9.65 (s, 1H, CONH), 7.85 – 7.83 (dd, *J* = 4.5, 4.0 Hz, 4H, Ar-H), 7.65 – 7.62 (m, 1H, Ar-H), 7.60 – 7.57 (t, *J* = 7.7 Hz, 2H, Ar-H), 7.22 – 7.21 (d, *J* = 8.4 Hz, 2H, Ar-H), 7.15 – 7.13 (d, *J* = 8.0 Hz, 1H, Ar-H), 7.05 (s, 1H, Ar-H), 6.99 – 6.98 (d, *J* = 8.0 Hz, 1H, Ar-H), 2.26 (s, 3H, CH_3), 2.14 (s, 3H, CH_3). ^{13}C NMR (125 MHz, DMSO-d6): δ = 164.98, 141.10, 139.80, 135.43, 134.25, 133.93, 133.64, 131.26, 130.14, 129.90, 129.38, 127.16, 126.93, 118.82, 20.99, 18.28. MS (EI+): *m/z* calculated for $C_{21}H_{20}N_2O_3S$ 380.46, found – 380.47 (M^+).

***N-(3,5-dimethylphenyl)-4-(phenylsulfonamido) benzamide* (53)**

Brown solid (0.203 g, 59.19 % yield). M.P.: 180 –184˚C, R_f = 0.44 (EA/Hex, 4:6, v/v). IR (ATR): 3257 (secondary NH stretching), 1642 (C=O stretching), 1337 (asymm. S=O stretching) and 1158 (symm. S=O stretching) cm^{-1}. ^1H NMR (500 MHz, DMSO-d6): δ = 10.75 (s, 1H, SO_2NH), 9.93 (s, 1H, CONH), 7.85 – 7.83 (d, *J* = 7.3 Hz, 2H, Ar-H), 7.81 – 7.79(d, *J* = 8.6 Hz, 2H, Ar-H), 7.64 – 7.62 (d, *J* = 7.2 Hz, 1H, Ar-H), 7.60 – 7.57 (m, 2H, Ar-H), 7.34 (s, 2H, Ar-H), 7.22 – 7.20 (d, *J* = 8.6 Hz, 2H, Ar-H), 6.72 (s, 1H, Ar-H), 2.24 (s, 6H, 2 X CH_3). ^{13}C NMR (125 MHz, DMSO-d6): δ = 165.08, 139.78, 137.92, 133.64, 129.89, 129.40, 129.38, 127.15, 118.76, 118.50, 118.48, 21.58. MS (EI+): *m/z* calculated for $C_{21}H_{20}N_2O_3S$ 380.46, found – 380.46 (M^+).

***N-(2-ethylphenyl)-4-(phenylsulfonamido) benzamide* (54)**

Cream solid (0.289 g, 84.26 % yield). M.P.: 185 – 188˚C, R_f = 0.4 (EA/Hex, 4:6, v/v). IR (ATR): 3117 (secondary NH stretching), 1644 (C=O stretching), 1331 (asymm. S=O stretching) and 1158 (symm. S=O stretching) cm^{-1}. ^1H NMR (500 MHz, DMSO-d6): δ = 10.75 (s, 1H, SO_2NH), 9.73 (s, 1H, CONH), 7.85 – 7.84 (m, 4H, Ar-H), 7.64 – 7.57 (m, 3H, Ar-H), 7.28 – 7.19 (m, 6H, Ar-H), 2.58 – 2.55 (q, *J* = 7.5 Hz, 2H, CH_2), 1.11 – 1.08 (t, *J* = 7.6 Hz, 3H, CH_3). ^{13}C NMR (125 MHz, DMSO-d6): δ = 165.36, 141.17, 140.22, 139.81, 136.22, 133.65, 130.04, 129.91, 129.39, 128.89, 127.94, 127.16, 126.88, 126.43, 118.82, 24.37, 14.56. MS (EI+): *m/z* calculated for $C_{21}H_{20}N_2O_3S$ 380.46, found – 350.44 (M^+).

***N-(4-methyl-2-nitrophenyl)-4-(phenylsulfonamido) benzamide* (55)**

Yellow solid (0.245 g, 66.05 % yield). M.P.: 179 – 183˚C, R_f = 0.47 (EA/Hex, 4:6, v/v). IR (ATR): 3219 (secondary NH stretching), 1666 (C=O stretching), 1338 (asymm. S=O stretching) and 1156 (symm. S=O stretching) cm^{-1}. ^1H NMR (500 MHz, DMSO-d6): δ = 10.83 (s, 1H, SO_2NH), 10.51 (s, 1H, CONH), 7.87 – 7.79 (m, 5H, Ar-H), 7.65 – 7.53 (m, 5H, Ar-H), 7.25 (d, *J* = 8.7 Hz, 2H, Ar-H), 2.38 (s, 3H, CH_3). ^{13}C NMR (125 MHz, DMSO-d6): δ = 164.98, 143.18, 141.80, 139.70, 135.96, 134.95, 133.72, 129.92, 129.57, 129.48, 128.98, 127.16, 126.32, 125.27, 118.83, 20.51. MS (EI+): *m/z* calculated for $C_{20}H_{17}N_3O_5S$ 411.43, found – 411.03 (M^+).

***N-methyl-4-(phenylsulfonamido) benzamide* (63)**

Brown yellow solid (0.180 g, 68.76 % yield). M.P.: 159 – 163˚C, R_f = 0.49 (EA/Hex, 4:6, v/v). IR (ATR): 3152 (secondary NH stretching), 1659 (C=O stretching), 1308 (asymm. S=O stretching) and 1158 (symm. S=O stretching) cm^{-1}. ^1H NMR (500 MHz, DMSO-d6): δ = 10.66 (s, 1H, SO_2NH), 8.29 (s, 1H, CONH), 7.81(s, 2H, Ar-H), 7.70(s, 2H, Ar-H), 7.62 – 7.79 (d, *J* = 28.3 Hz, 3H, Ar-H), 7.16 (s, 2H, Ar-H), 2.73 (s, 3H, CH_3).

^{13}C NMR (125 MHz, DMSO-d6): δ = 165.83, 140.12, 139.21, 133.02, 129.67, 129.59, 129.27, 128.18, 127.97, 126.57, 118.35, 26.06. MS (EI+): *m/z* calculated for $C_{14}H_{14}N_2O_3S$ 290.34, found – 290.43 (M^+).

***N-ethyl-4-(phenylsulfonamido) benzamide* (64)**

Brown yellow solid (0.164 g, 60.12 % yield). M.P.: 163 –166˚C, R_f = 0.47 (EA/Hex, 4:6, v/v). IR (ATR): 3140 (secondary NH stretching), 1633 (C=O stretching), 1307 (asymm. S=O stretching) and 1158 (symm. S=O stretching) cm^{-1}. ^{1}H NMR (500 MHz, DMSO-d6): δ = 10.65 (s, 1H, SO_2NH), 8.31 (s, 1H, CONH), 7.81 – 7.80 (d, *J* = 7.7 Hz, 2H, Ar-H), 7.70 – 7.69 (d, *J* = 7.9 Hz, 2H, Ar-H), 7.63 – 7.54 (dt, J_1 = 30 Hz, J_2 = 7.2 Hz, 3H, Ar-H), 7.16 – 7.14 (d, *J* = 7.9 Hz, 2H, Ar-H), 3.25 – 3.20 (q, J_1 = 13 HZ, J_2 = 6.5 Hz, 2H, CH_2), 1.09 – 1.06 (t, *J* = 7.0 Hz, 3H, CH_3). ^{13}C NMR (125 MHz, DMSO-d6): δ = 165.12, 140.08, 139.18, 133.00, 130.63, 129.83, 129.25, 128.23, 126.56, 118.35, 118.05, 14.69. MS (EI+): m/z calculated for $C_{15}H_{16}N_2O_3S$ 290.34, found – 290.43 (M^+).

***N-butyl-4-(phenylsulfonamido) benzamide* (65)**

Brown solid (0.189 g, 63.06 % yield). M.P.: 171 –174˚C, R_f = 0.42 (EA/Hex, 4:6, v/v). IR (ATR): 3152 (secondary NH stretching), 1630 (C=O stretching), 1309 (asymm. S=O stretching) and 1156 (symm. S=O stretching) cm^{-1}. ^{1}H NMR (500 MHz, DMSO-d6): δ = 10.65 (s, 1H, SO_2NH), 8.28 (s, 1H, CONH), 7.81 – 7.80 (d, *J* = 7.0 Hz, 2H, Ar-H), 7.70 – 7.69 (d, *J* = 7.3 Hz, 2H, Ar-H), 7.63 – 7.56 (dt, J_1 = 22.5 Hz, J_2 = 6.2 Hz, 3H, Ar-H), 7.16 – 7.14 (d, *J* = 7.3 Hz, 2H, Ar-H), 3.25 – 3.20 (q, *J* = 7.3 Hz, 2H, CH_2), 1.48 – 1.41 (p, *J* = 7.75 Hz, 2H, CH_2), 1.34 – 1.23 (hex , *J* = 7 Hz, 2H, CH_2), 0.88 – 0.85 (t, *J* = 8 Hz, 3H, CH_3). ^{13}C NMR (125 MHz, DMSO-d6): δ = 165.28, 140.09, 139.22, 133.01, 129.87, 129.27, 128.27, 126.58, 118.33, 38.91, 31.16, 19.54, 13.61. MS (EI+): *m/z* calculated for $C_{18}H_{19}N_2O_3S$ 332.42, found – 332.47 (M^+).

***N, N-dimethyl-4-(phenylsulfonamido) benzamide* (66)**

Brown solid (0.162 g, 59.03 % yield). M.P.: 175 – 177˚C, R_f = 0.43 (EA/Hex, 4:6, v/v).IR (ATR): 3145 (secondary NH stretching), 1626 (C=O stretching), 1319 (asymm. S=O stretching) and 1157 (symm. S=O stretching) cm^{-1}. ^1H NMR (500 MHz, DMSO-d6): δ = 10.58 (s, 1H, SO_2NH), 8.28 (s, 1H, CONH), 7.81 – 7.80 (s, *J* = 6 Hz, 2H, Ar-H), 7.62 – 7.56 (m, 3H, Ar-H), 7.30 – 7.28 (d, *J* = 6.7 Hz, 2H, Ar-H), 7.14 – 7.13 (d, *J* = 7.0 Hz, 2H, Ar-H), 2.91 –2.85 (d, *J* = 30 Hz, 3H, CH_3). ^{13}C NMR (125 MHz, DMSO-d6): δ = 13C NMR (126 MHz, DMSO) δ 169.43, 139.30, 138.61, 132.98, 131.48, 129.26, 128.24, 126.54, 118.69, 39.91, 39.74, 39.57, 39.41, 39.24, 39.07, 38.91, 34.70. MS (EI+): *m/z* calculated for $C_{15}H_{16}N_2O_3S$ 304.36, found – 304.39 (M^+).

***N, N-dimethyl-4-(phenylsulfonamido) benzamide* (67)**

Brown solid (0.185 g, 61.72 % yield). M.P.: 176 – 179˚C, R_f = 0.40 (EA/Hex, 4:6, v/v). IR (ATR): 3155 (secondary NH stretching), 1632 (C=O stretching), 1342 (asymm. S=O stretching) and 1155 (symm. S=O stretching) cm^{-1}. ^1H NMR (500 MHz, DMSO-d6): δ = 10.61 (s, 1H, SO_2NH), 8.29 (s, 1H, CONH), 7.80 – 7.78 (s, *J* =10 Hz, 2H, Ar-H), 7.62 – 7.56 (m, 3H, Ar-H), 7.30 – 7.28 (dd, J_1 = 24.9 Hz, J_2 = 5 Hz, 4H, Ar-H), 3.11 (s, 4H, CH_2), 1.05 (s, 6H, CH_3). ^{13}C NMR (125 MHz, DMSO-d6): δ = 169.43, 139.30, 138.61, 132.98, 131.48, 129.26, 128.24, 126.54, 118.69, 34.31, 19.1. MS (EI+): *m/z* calculated for $C_{15}H_{16}N_2O_3S$ 332.42, found – 332.59 (M^+).

***N-hydroxy-4-(phenylsulfonamido) benzamide* (68)**

Brown solid (0.120 g, 45.53 % yield). M.P.: 156 – 158˚C, R_f = 0.20 (EA/Hex, 4:6, v/v). IR (ATR): 3245 (secondary NH stretching), 1654 (C=O stretching), 1312 (asymm. S=O stretching) and 1159 (symm. S=O stretching) cm^{-1}. ^1H NMR (500 MHz, DMSO-d6): δ = 10.62 (s, 1H, SO_2NH), 10.23 (s. 1H, OH), 8.07 (s, 1H, CONH), 7.81(s, 2H, Ar-H), 7.73(s, 2H, Ar-H), 7.78 – 7.61 (d, *J* = 28 Hz, 3H, Ar-H), 7.13 (s, 2H, Ar-H). ^{13}C NMR (125 MHz,

DMSO-d6): δ = 176.23, 139.31, 138.63, 131.90, 131.48, 129.17, 128.64, 126.51, 117.29. MS (EI+): m/z calculated for $C_{13}H_{12}N_2O_4S$ 292.31, found – 292.51 (M^+).

***N-(4-(hydrazinecarbonyl)phenyl) benzene sulfonamide* (69)**

Brown solid (0.090 g, 34.26 % yield). M.P.: 212 – 218˚C, R_f = 0.18 (EA/Hex, 4:6, v/v). IR (ATR): 3256 (secondary NH stretching), 1658 (C=O stretching), 1319 (asymm. S=O stretching) and 1157 (symm. S=O stretching) cm^{-1}. ^1H NMR (500 MHz, DMSO-d6): δ = 10.56 (s, 1H, SO_2NH), 9.12 (s. 1H, NH), 8.15 (s, 1H, CONH), 7.81(s, 2H, Ar-H), 7.73(s, 2H, Ar-H), 7.79 – 7.62 (d, *J* = 28 Hz, 3H, Ar-H), 7.14 (s, 2H, Ar-H). ^{13}C NMR (125 MHz, DMSO-d6): δ = 171.59, 138.28, 138.12, 131.89, 131.56, 129.27, 128.64, 126.41, 117.10. MS (EI+): *m/z* calculated for $C_{13}H_{12}N_2O_4S$ 291.33, found – 291.71 (M^+).

***methyl-4-(phenylsulfonamido) benzamide* (73)**

Crimson pink solid (0.249 g, 94.80 % yield). M.P.: 158 – 163˚C, R_f = 0.5 (EA/Hex, 4:6, v/v). IR (ATR): 3219 (secondary NH stretching), 1691 (C=O stretching), 1337 (asymm. S=O stretching) and 1154 (symm. S=O stretching) cm^{-1}. ^1H NMR (500 MHz, DMSO-d6): δ = 10.66 (s, 1H, SO_2NH), 7.84 – 7.80 (t, *J* = 10 Hz, 4H, Ar-H), 7.63 – 7.60 (t, *J* = 7.5 Hz, 1H, Ar-H), 7.56 – 7.54 (t, *J* = 7.5 Hz, 3H, Ar-H), 7.21 – 7.20 (s, *J* = 8 Hz, 2H, Ar-H), 3.76 (s, 3H, CH_3). ^{13}C NMR (125 MHz, DMSO-d6): δ = 166.17, 143.71, 140.07, 133.51, 131.04, 129.81, 127.10, 124.45, 118.75, 109.31, 52.34. MS (EI+): *m/z* calculated for $C_{14}H_{13}NO_4S$ 291.32, found – 291.43 (M^+).

***ethyl-4-(phenylsulfonamido) benzamide* (74)**

Crimson pink solid (0.260 g, 94.44 % yield). M.P.: 160 – 164˚C, R_f = 0.49 (EA/Hex, 4:6, v/v). IR (ATR): 3227 (secondary NH stretching), 1688 (C=O stretching), 1334 (asymm. S=O stretching) and 1155 (symm. S=O stretching) cm^{-1}. ^1H NMR (500 MHz, DMSO-d6): δ = 10.88 (s, 1H, SO_2NH), 7.83 (s, 4H, Ar-H), 7.63 – 7.58 (d, *J* = 25 Hz, 3H, Ar-H),

7.24 (4, 2H, Ar-H), 4.26 – 4.21 (q, *J* = 7.5 Hz, 2H, Ar-H), 1.27 – 1.24 (t, *J* = 8 Hz, 3H, CH_3). ^{13}C NMR (125 MHz, DMSO-d6): 165.04, 142.19, 139.11, 133.17, 130.50, 129.35, 126.61, 124.64, 118.13, 60.41, 14.07. MS (EI+): *m/z* calculated for $C_{15}H_{15}NO_4S$ 305.35, found – 305.62 (M^+).

***n-butyl-4-(phenylsulfonamido) benzamide* (75)**

Crimson pink solid (0.260 g, 86.49 % yield). M.P.: 172 – 174˚C, R_f = 0.43 (EA/Hex, 4:6, v/v). IR (ATR): 3235 (secondary NH stretching), 1689 (C=O stretching), 1324 (asymm. S=O stretching) and 1157 (symm. S=O stretching) cm^{-1}. ^{1}H NMR (500 MHz, DMSO-d6): δ = 10.89 (s, 1H, SO_2NH), 7.83 (s, 4H, Ar-H), 7.62 – 7.57 (d, *J* = 25 Hz, 3H, Ar-H), 7.24 (4, 2H, Ar-H), 4.2 – 4.17 (t, *J* = 10 Hz, 2H, Ar-H), 1.63 – 1.60 (t, *J* = 8.5 Hz, 2H, CH_2), 1.38 – 1.33 (p, *J* = 8.5 Hz, 2H, CH_2), 0.9 – 0.86 (p, *J* = 9 Hz, 3H, CH_3). ^{13}C NMR (125 MHz, DMSO-d6): 165.09, 142.24, 139.17, 133.18, 130.51, 129.36, 126.62, 124.61, 118.14, 64.07, 30.17, 18.64, 13.50. MS (EI+): *m/z* calculated for $C_{17}H_{19}NO_4S$ 333.40, found – 333.89 (M^+).

4.2.3. *In vitro* cholinesterase inhibitory activity

Ellman's method was used to carry out the *in vitro* BChE and AChE inhibition studies of the synthesised compounds [189, 190]. Equine BChE and *Electrophorus electricus* AChE (CAS No. 9000-81-5 and 9001-08-1) were procured from Sigma Aldrich, *acetylthiocholine iodide* (ATCI, CAS No. 1866-15-5), *butyrylthiocholine iodide* (BTCI, CAS No. 1866-16-6), *5,5'-dithiobis(2-nitrobenzoic acid)* (DTNB, CAS No. 69-78-3) were purchased from Himedia. Compounds (**3**, **30** – **56**, **63** – **69**, **73** – **75**) were initially screened for AChE and BChE inhibition at a concentration of 50 μM. Further, the compounds producing promising % inhibition were screened to determine their IC_{50}. Six concentrations of inhibitors, i.e., 50, 500, 1000, 5000, 10000 and 50000 nM, were prepared from a stock solution of 1 mg/ml in methanol by taking care of the dilutions in

the assay solution. The enzyme assays were performed in phosphate buffer saline (PBS, pH 7.4). Initially, 10 µL of working solutions of inhibitors and 100 µL of DTNB solution (0.005 M) prepared in PBS were mixed in a 96 well plate and were incubated for 10 min. After incubation,50 µL of AChE (0.5 U mL^{-1}) or 50 µL of BChE (0.5 U mL^{-1}) was added, and was followed by further incubation for 15 min. Finally, 30 µL substrate, i.e., ATCI (0.00235 M,) or BTCI (0.00235 M) prepared in PBS, was added to the reaction mixture. The formation of yellow coloured 5-*thio-2-nitrobenzoate* anion was measured at 1 min interval for 20 min at absorbance of 415 nm on Synergy HTX multimode reader (BioTek, USA), against a blank containing 10 µL methanol instead of test compound and performed in triplicate [191]. The IC_{50} was determined using GraphPad Prism 5.

The enzyme kinetics was performed for compounds **34** and **37,** based on their IC_{50} values, to determine the mechanism of inhibition. Five different concentrations of the inhibitor, i.e., 15, 30, 60, 120 and 240 nM of compound **34** and 10.5, 21, 42, 84 and 168 nM of compound **37,** were used for enzyme kinetic study. The criteria for selection of the concentrations were, two concentrations higher and two concentrations lower than the IC_{50} of the compounds. Each inhibitor concentration was incubated with six different concentrations of BTCI, i.e., 0.25, 1, 2, 3, 4 and 5 µM. The absorbance of the reaction mixture was recorded at 415 nm for 25 min on Synergy HTX multimode reader (BioTek, USA) against a blank containing 10 µL methanol instead of the test compound. The velocity of the enzyme obtained from the product formed was used to calculate V_{max}, K_m by Michaelis-Menten nonlinear regression graph and mechanism of enzyme inhibition by Lineweaver-Burk reciprocal plots. The Ki value was obtained from the Dixon plot of the slope of the double reciprocal Lineweaver-Burk plot vs concentrations of test compounds. The enzyme kinetic assay was performed in triplicate [192].

4.2.4. *In vitro* blood-brain barrier permeation assay

Porcine brain lipid (PBL, CAS No. 475995-51-8) and dodecane were obtained from Avanti polar lipids, Alabaster and Avra Synthesis, Hyderabad, respectively. The donor and acceptor with PVDF membrane (pore size 0.45 mm) microplates (Cat No. MAIPNTR10 and MATRNPS50) were purchased from Merck Millipore. The BBB permeability was determined by the parallel artificial membrane permeation assay (PAMPA) of compounds **34, 37** and **55** [193]. The acceptor plate was coated with 4 µL of 20 mg/ml PBL in dodecane, followed by hydration with 200 µL of PBS (pH 7.4). The working solution of 25 µg/ml of each compound was prepared by a 200-fold dilution of 5 mg/mL stock solution in DMSO with PBS (pH 7.4). Further, 200 µL of working solution were added to each well of the donor plate. The donor was placed over acceptor plates followed by incubation for 18 h. The concentration of the compound in the acceptor, donor and reference wells were determined by UV spectroscopy (HTX multimode reader, BioTek, USA). Each sample was scanned for at least five different wavelengths and in three independent runs. In our previous study, the protocol was already validated by using nine commercial drugs (Verapamil, Diazepam, Progesterone, Atenolol, Dopamine, Lomefloxacin, Alprazolam, Chlorpromazine and Oxazepam) with known BBB permeability [147].

$$P_e = \left(\frac{(V_D - V_A)}{(V_D + V_A)a \times t}\right) \times ln\left(1 - \frac{[Drug]_{acceptor}}{[Drug]_{equilibrium}}\right)$$

4.2.5. Cell viability (MTT Assay)

The human neuroblastoma (SH-SY5Y) cells, procured from National Centre for Cell Science (Pune, India), were grown in minimum essential media (MEM) with 10% foetal bovine serum as a supplement at 37 °C and an atmosphere containing 5% CO_2 in an incubator (Heal force, Germany). Further, the cells were trypsinated, washed and resuspended in MEM to obtain 5 X 10^4 cells/well in the 96 well plates. Five different

dilutions of compounds (2, 10, 20, 50 and 100 µM) were prepared in DMSO and incubated for 24 h. At the end of incubation period, the cells were again incubated for 4 h with 5 µL of (3-(4,5-dimethylthiazol-2-yl)-2,5-diphenyltetrazolium bromide (MTT) (5 mg/ml). Formazan crystals were dissolved in 150 µL of dissolving solvent (DMSO: H_2O, 1:1), after gently removing culture media from wells. The absorbance was immediately recorded at 570 nm by UV spectroscopy (HTX multimode reader, BioTek, USA). The response was expressed as percentage cell viability in triplicate [147, 194].

4.2.6. *In silico* ADMET and molecular property analysis

The *in silico* ADMET and molecular properties were determined by Biosigs's pkCSM web-server (http://biosig.unimelb.edu.au/pkcsm/prediction) using SMILES strings of the compounds [195].

4.2.7. Molecular docking

The 3D coordinates of ligands were generated using Rdkit from the SMILES strings of the compounds. It was followed by energy minimisation using MMFF94s forcefield and were converted into Mol2 using Open Babel. Finally, the ligands were converted to PDBQT format by Autodock Tools-1.5.6, respectively. The grid maps were generated for atoms (A, C, HD, NA, N, OA, S, Br, Cl and I) present in the ligands with a grid box of dimension 78 × 90 × 86 and grid centre was placed at 55.007, 53.553 and 43.81 representing X, Y and Z coordinates, respectively. The grid point spacing of 0.375 Å was maintained. A Lamarckian genetic algorithm and Solis-Water local search were used for docking on horse BChE, obtained by homology modelling through Autodock-4.2.6. The docking results were obtained from a python script, i.e., vstools_v0.16, and visualisation was performed by Discovery studio visualiser 2020 [196, 197].

4.2.8. QSAR

The QSAR of the synthesised sulfonamide derivatives (**scheme 1**) was performed using python-3.7.6. The IC_{50} values were converted to PIC_{50} values for the development of

various models. 150 CATS2D and 1452 2D descriptors obtained from the PyBioMed package and Mordred server, respectively, were used to develop two separate QSAR models [187, 198]. Each dataset was divided into training and test sets and chemical similarity amount both sets were ensured. Decision tree-based regression and linear regression were employed on Mordred and CATS2D descriptors for the development of QSAR models. The descriptors with zero variance as well as highly correlated descriptors were dropped. A feed-forward feature selection was carried out using mlxtend python package in order to obtain a set of fifteen most relevant descriptors. The models were developed by using various subsets of features. The evaluation criteria used were determination coefficient (r^2), MAE and MSE for initial models. The descriptor combinations, that performed well, were again subjected to internal validation using the leave- one- out (LOO) strategy and finally tested on the test set. The leave-one-out cross-validated correlation coefficient (Q^2_{LOO}), MAE_{LOO}, MSE_{LOO} and r_m^2 metrics like average r_m^2 and Δr_m^2 were calculated. The external validation on the test set were carried out using Q^2ext-based metrics (Q^2_{F1} and Q^2F_2), MAE, MSE and r_m^2 metrics [199].

4.2.9. Molecular dynamics

The ligand poses obtained were parameterised through Antechamber using general AMBER force field (GAFF2) and the Austin model with bond and charge correction (AM-BCC1) atomic partial charges. The topologies and coordinates of protein and protein-ligand complexes were build using *tleap* module of AMBER 20. The complexes were hydrated with TIP3P water molecules in a cubic box with a cut-off distance of 12 Å between any atom initially present in solute and the edge of the periodic boundary and neutralised by adding Na+ and Cl- ions. The systems were subjected to energy minimisation, heating, density equilibration and equilibration under periodic boundary conditions [197, 200]. The final 50 ns MD productions were carried out at 310.15 K as

an NPT ensemble [201-203]. Further, the post MD processing was carried out using *cpptraj*.

4.2.10. *In vivo* evaluation of compounds

4.2.10.1. Drugs and treatments

Male Wister rats weighing 150 – 200 g were selected for the study. Six rats were kept in each polyacrylic cage with a 12-hour light/dark cycle at a regulated temperature (25 ± 2 °C) and humidity (50 ± 10%). The animals were given free access to food and water and were acclimatised for one week prior to the experiment. The food was withheld one hour before the behavioural trial. The experimental protocols were approved by the Institutional Animal Ethics Committee of the Banaras Hindu University, Varanasi, India (Dean/2021/IAEC/2565). Scopolamine hydrobromide (SCO) was used to induced amnesia at a dose of 5 mg/Kg. The animals were segregated into nine groups, with six animals in each group. The following treatments were used in the study: (I) control, (II) SCO (5 mg/Kg), (III) SCO + donepezil (5 mg/Kg), (IV) SCO + compound **34** (5 mg/Kg), (V) SCO + compound **34** (10 mg/Kg), (VI) SCO + compound **34** (20 mg/Kg), (VII) SCO + compound **37** (5 mg/Kg), (VIII) SCO + compound **37** (10 mg/Kg), and (IX) SCO + compound **37** (20 mg/Kg). Donepezil and SCO were dissolved in distilled water, while the investigational compounds were suspended in 0.5% SCMC prior to the administration. SCO was administered through intraperitoneal injection (i.p.) and other compounds were administered through the oral route (p.o.) using oral gavage. The compounds, except SCO, were administered for seven days, while SCO was administered on the seventh day to induce amnesia. The behavioural experiments were performed half-hour after the SCO administration [204].

4.2.10.2. LD_{50} determination

Compounds **34** and **37** were initially tested for determining LD_{50}, using OECD guideline 423 – acute toxicity class method. The compounds were tested for 500 and 2000 mg/Kg

doses with three female Wistar rats in each group. The animals were administered doses, followed by observation for 72 h (**Table T2 -T13 in appendix**). LD_{50} of the compounds was calculated according to the guideline [205].

4.2.10.3. Y-maze test

Y-maze is an apparatus with three identical wooden arms (A, B and C), that are separated by 120˚ angle. It is used to evaluate the intermediate working and spatial memory. The test compounds **34, 37** and donepezil were evaluated on the seventh day of the treatment. Initially, a training session was carried out in which one of the arms was closed by using a wooden partition, and the animal was allowed to enter the maze with the head facing towards the centre. The training was performed after the dosing and four hours prior to the test session, and the animal was allowed to explore the maze for 15 minutes. The test session was carried out after half an hour of administration of SCO. In this session, the novel arm was opened, and the rodent could move in the maze freely for five minutes. The series of arm entries were recorded. The repetition of entries in the same arm indicated memory impairment. The novel arm entries and the spontaneous alteration in the three-consecutive components (ABC, BCA, CAB, not ABA) was considered as the sign of memory improvement [206, 207]. The maze was cleaned with 70 % of ethanol after each session to remove any olfactory clues. The % spontaneous alteration was calculated as:

$$\%\ Spontaneous\ alteration = \frac{Number\ of\ alteration}{(total\ arm\ entries - 2)} \times 100$$

4.2.10.4. Barnes maze

The Barnes maze consists of 20 holes with 10 cm diameter uniformly distributed on the periphery of a grey wooden circular platform of 122 cm in diameter and raised 100 cm

above the ground. The platform is illuminated by white light with a luminous intensity of more than 600 lux and a sound higher than 80 dB was used with the help of a siren.

Habituation

The phase involved habituation to the platform and the escape box of the maze to reduce anxiety in the rats. It was performed a day before the acquisition phase. The animals were habituated for three minutes in presence of light and absence of noise.

Acquisition phase

The acquisition phase consisted of one session per day for five consecutive days. Each session had two trials of 180 seconds each at an interval of 15 minutes. The training started by placing an animal on the centre of the platform and was covered by a black box. It was followed by turning on the light and sound sources, and the animal was released after 10 seconds. The animal was allowed to explore the maze and identify the location of the escape box using visual clues. As the rodent entered the hole of the escape box, the entrance of the hole was covered and the light and sound stimuli were turned off. The animal was allowed to stay in the box for 30 seconds and then returned to the cage. If the animal was unable to find the escape box within 180 seconds, it was gently guided to the escape box and the animal was allowed to explore the box for 30 seconds. All the olfactory stimuli were cleaned with 70 % ethanol. Primary latency and primary errors were recorded. Primary latency is the time required for a rat to reach the escape box, while primary errors are defined as the number of holes visited by the animal before finding the escape hole.

Probe trial

The probe trial was conducted on the seventh day of the treatment, 30 minutes after i.p. administration of the SCO. It was conducted in a similar manner with the escape hole

closed. The rat was allowed to explore the maze for 90 seconds, and primary latency and errors were recorded [208, 209].

4.2.10.5. Neurochemical analysis

The animals were euthanised after the experiments followed by removal of the brains. The hippocampus and prefrontal cortex (PFC) were used for the neurochemical analysis. The tissue was homogenised in 10 mM of phosphate buffer saline (PBS; pH 7.4) and centrifuged at 15000 rpm for 15 minutes at 4˚ C. The supernatant was collected and used for further analysis. ChE activity was measured with the help of acetylthiocholine iodide (ATCI) and butyrylthiocholine iodide (BTCI) by Ellman method. Firstly, 10 µL of the supernatant was diluted with 100 µL of the PBS, followed by the addition of freshly prepared 50 µL of substrate solutions (5 mM) and incubated for 5 minutes. It was followed by the addition of 1.5 mM of DTNB solution, and absorbance was recorded at 415 nm on Synergy HTX multimode reader (BioTek, USA) against a blank.

The catalase (CAT) enzyme is responsible for the conversion of harmful H_2O_2 into water and oxygen. CAT activity in tissue homogenate was measured by mixing 10 µL of supernatant with 150 µL of PBS. It was followed by the addition of 250 µL of H_2O_2 (160 mM) and incubation of 1 minute at 37 ˚C. Further, 1.5 mL of stopping solution of dichromate/acetic acid solution (5% $K_2Cr_2O_7$/glacial acetic acid; 1:3 v/v) was added, and the reaction mixture was boiled for 15 min. The green colour appearing due to the oxidation of dichromate to chromic (III) sulfate was compared with the control mixture, containing all the components except the enzyme. The absorbance was recorded at 570 nm on Synergy HTX multimode reader (BioTek, USA) against a blank [147]. Superoxide dismutase (SOD) was measured using Markland's method, based on the autoxidation of pyrogallol. In 10 µL of the tissue homogenate, 200 µL of 0.l M of Tris-HCl with 1 mM EDTA at pH 8.2 were added. It was followed by the addition of 50 µL of 4.5 mM of

pyrogallol solution prepared in 1 µM of HCl. The absorbance was measured after 1 minute at 325 nm wavelength on Synergy HTX multimode reader (BioTek, USA) against a blank. A control sample, without tissue supernatant, was used to determine the enzyme activity. The experiments were performed in triplicates, and enzyme activities were normalised with respect to the control group.

4.2.10.6. Biochemical analysis

Alanine Aminotransferase (ALT/SGPT), Aspartate Aminotransferase (AST/SGOT), urea and creatinine were determined in the serum of animals treated with compounds (**34** and **37)** and control using a commercially available kit obtained from Tara clinical system.

4.2.10.7. Statistical analyses

All values were expressed as the mean ± standard error of the mean (SEM). One-way ANOVA followed by Newman-Keuls multiple comparison posthoc test was performed.

4.3. Results and discussion

4.3.1. Development of machine learning models and prediction of BChE inhibitors

The dataset of BChE inhibitors was obtained from ChEMBL database has 3892 compounds. The 613 and 421 inhibitors were removed due to unreported IC_{50} values and duplicate entry, respectively. The objective of the study was identification of BChE inhibitors for AD; hence the compounds impermeable to BBB would be futile. A molecular properties-based filter, to determine BBB permeability, was applied with criteria: molecular weight < 450, logP < 5, H-bond donor < 3, H-bond acceptor < 7, number of rotatable bonds < 8, total number of H-bonds < 8, pKa (neutral or basic) 7.5–10.5 and polar surface area < 70 Å was applied, which resulted in 2517 compounds. The compounds were divided into various subsets as indicated in **Figure 4.1**. A set of 765 two dimensional descriptors were calculated from Pybiomed. The other datasets were prepared from Daylight, MACCS and ECFP4 fingerprints. A correlation filter was

applied to each dataset to obtain final features (**Figure 4.1**). It was followed by feature normalisation, i.e., all features were scaled between 0 to 1. ML algorithms like LR, SVM, ridge classifier and perceptron use gradient descent technique to identify the minima. The values of various features on different unit scale adversely affect the process. Hence, feature scaling ensures gradient descent at a similar rate for all the variables. The normalisation is also important in the case of the KNN algorithm, which solely depends upon the distance and features. The higher magnitude would have more impact on the model and create a bias towards that feature(s). Feature scaling was not required for the remaining algorithms used in the study. BChE inhibitor dataset had a class imbalance in compound distribution. Hence, the adjusted weight of each class was set to an inverse of the number of samples present in a class. The models were trained using 5-fold validation and mean training accuracies were used in model selection. The hyperparameter tuning resulted in numerous models, and one model per algorithm was selected for each dataset. The selected models are presented in **Figure 4.2**. The selection criteria for models included the mean training and validation accuracies should be above 85%. The accuracy of training set clearly indicated that RF, bagging and GB classifiers performed well on the training set for all the descriptor sets. In case of the validation dataset, it was observed that all the three algorithms did not meet the criteria for MACCS datasets. The adaboost classifier displayed good performance only on the daylight training dataset. On contrary, the validation performance of the classifier was more than 85 % for Pybiomed and ECFP4 datasets. In case of KNN classifier, the desired accuracies could only be achieved on Pybiomed descriptors datasets.

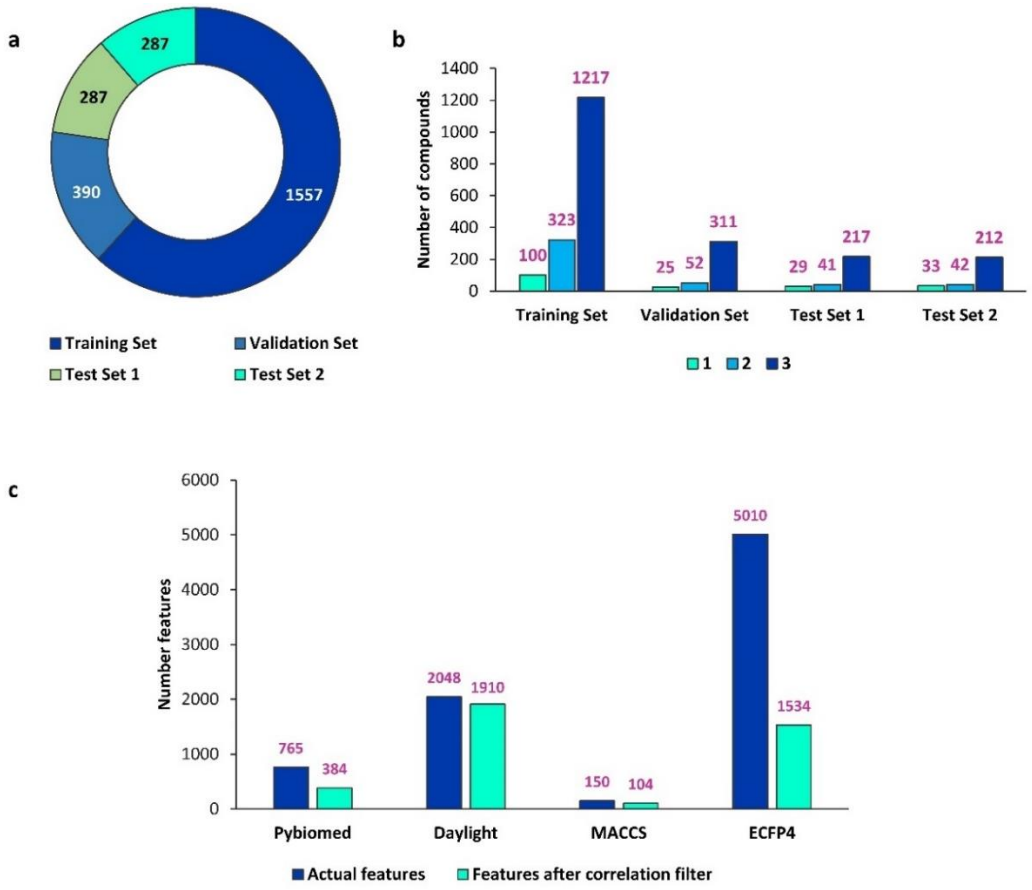

Figure 4.1 Sample distribution of compounds (a) among various datasets. (b) based on class labels across (c) Number of features before and after data processing.

However, the selection of models only on the basis of accuracy is not suitable due to accuracy paradox. The accuracy is unsuitable predictive metric, when sample distribution among the classes is unbalanced, i.e., one of the classes dominates the others. In such sample distribution, higher accuracy is observed. The other metrics, viz. precision and recall are preferred. However, in some instances, precision is also biased towards the unbalanced class. The use of F1 metrics, which is a harmonic mean of the precision and recall, is helpful. A good model aims at high precision and recall values, which is quite difficult to achieve for a model. It was observed that eight out of ten final models displayed F1 score higher than 85 %. The models also displayed recall and precision values greater than 85 %, indicating a good precision-recall balance.

a

Algorithm	Pybiomed	Daylight	MACCS	ECFP4
Logistic Regression	81.01	84.05	79.87	84.2
Support Vector Classifier	80.3	81.3	79.49	83.3
K-Nearest Nieghbour	85.32	86.23	83.22	85.29
Ridge Classifier	72.63	80.46	69.84	80.67
Perceptron	70.57	80.91	76.91	81.57
Linear Discriminant Analysis	81.39	61.89	81.86	76.62
Quadratic Discriminent Analysis	77.66	20.12	40.45	61.01
Bernouolli Naïve Bayes	74.5	64.13	73.12	80.47
Label Propogation	83.64	84.18	83.6	83.17
Label Spreading	84.03	84.43	83.6	82.4
Passive Aggressive Classifier	65.31	83.34	76.21	77.2
Decision Tree Classifier	78.81	82.13	79.1	80.8
Random Forest Classifier	86.67	86.93	85.27	85.36
Bagging Classifeir	86.54	87.57	85.59	85.29
Gradient Boosting Classifer	86.41	87	85.47	85.42
AdaBoost Classifier	84.61	85.97	83.92	84.84

Training Set Accuracy

b

Algorithm	Pybiomed	Daylight	MACCS	ECFP4
Logistic Regression	80.21	82.61	80.72	82.82
Support Vector Classifier	79.18	79.8	80.21	83.08
K-Nearest Nieghbour	87.15	84.14	81.75	83.08
Ridge Classifier	69.67	80.05	71.98	80.51
Perceptron	80.46	79.8	60.67	82.31
Linear Discriminant Analysis	83.29	50.38	78.92	76.92
Quadratic Discriminent Analysis	81.49	20.46	32.9	65.13
Bernouolli Naïve Bayes	73.78	60.61	73.52	81.79
Label Propogation	81.23	84.65	82.01	86.15
Label Spreading	82.26	83.63	81.75	84.62
Passive Aggressive Classifier	23.65	83.89	69.41	82.82
Decision Tree Classifier	77.38	79.03	77.12	81.03
Random Forest Classifier	86.12	85.17	84.32	85.9
Bagging Classifeir	85.86	85.42	84.06	86.41
Gradient Boosting Classifer	86.89	86.45	82.52	85.9
AdaBoost Classifier	86.89	82.86	83.55	86.15

Validation Set Accuracy

$ Training accuracy is the mean representation and its standard deviation is reported in SI
$$ Descriptor : Pybiomed; Fingerprints : Daylight, MACCS and ECFP4

Figure 4.2 Accuracies of models on various datasets.

These selected models were further evaluated on test set 1 and 2. KNN models trained on Pybiomed dataset performed poorly on the test sets (**Table 4.1**). The RF model developed on ECFP4 dataset displayed inferior performance for all evaluation parameters on test set 2. RF-Daylight model displayed good performance on test set 2 and unsatisfactory performance on test set 1. The two bagging models also indicated inconsistent performance on test sets. The Pybiomed descriptor-based GB model displayed a

consistent performance on the test as well as validation sets and was selected for final prediction.

Table 4.1 Performance of the final models on training, validation, and test sets.

	Algorithm	**K-nearest neighbour**	**Bagging**	**Gradient boosting**	**Gradient boosting**	**Bagging**	**Random Forest**	**Random Forest**	**Gradient boosting**
	Descriptor	Pybiomed	ECFP4	Daylight	**Pybiomed**	Daylight	ECFP4	Daylight	ECFP4
Training Set	**Accuracy***	85.32 ± 0.82	85.29 ± 0.80	87.00 ± 2.30	**86.41 ± 1.83**	87.57 ± 1.09	85.36 ± 0.73	86.93 ± 1.51	85.42 ± 1.51
Validation Set	**Accuracy**	87.15	86.41	86.45	**86.89**	85.42	85.9	85.17	85.9
	Recall	87.15	86.41	86.45	**86.89**	85.42	85.9	85.17	85.9
	Precision	86.44	85.92	85.84	**85.35**	85.6	84.99	85.36	84.88
	F1 score	86.37	85.94	85.86	**85.62**	85.43	85.31	85.22	85.1
Test Set 1	**Accuracy**	70.73	83.97	82.93	**88.5**	83.62	84.32	83.28	83.62
	Recall	70.73	83.97	82.93	**88.5**	83.62	84.32	83.28	83.62
	Precision	75.41	83.15	81.52	**87.5**	82.59	84.72	82.37	83.16
	F1 score	72.35	83.06	81.76	**87.72**	82.74	83.77	82.64	82.22
Test Set 2	**Accuracy**	69.69	82.23	89.9	**86.41**	89.55	82.23	90.24	83.28
	Recall	69.69	82.23	89.9	**86.41**	89.55	82.23	90.24	83.28
	Precision	73.92	83.67	89.62	**85.38**	89.99	81.41	90.59	82.34
	F1 score	71.04	81.62	89.73	**85.2**	89.71	80.91	90.38	81.78

* Results are indicated in Mean ± SD.

Finally, the applicability domain was defined to ascertain reliable predictions made by the ML model. The applicability domain for the GB-Pybiomed descriptor-based ML model was defined through two criteria:

1. The molecules should meet the defined BBB permeability criteria.
2. If more than 5% of the Pybiomed descriptors of a test molecule lie outside the range (mean ± 1.5) of the training set, then the molecule should be rejected.

The prediction for a molecule that meets both criteria of the applicability domain could be considered reliable. In our previous studies, we obtained sulfonamide based inhibitors of AChE and BChE enzymes [147, 150]. Hence, a focused library of 300 sulfonamide compounds was developed from ZINC15 database [210]. The Pybiomed descriptors of the compounds were calculated and the applicability domain was applied. Twenty-one compounds passed the criteria and were subjected to binning process using ChemMinerR

[211]. This resulted in the identification of two series of compounds, and hence, their prototype compounds were used for prediction. Compounds **VH1** and **VH2** were identified as active and moderately active inhibitors, respectively (**Figure 4.3**). Compound **VH1**, a *4-amino benzoic acid* derivative, was selected and a library of amides and ester of *4-(phenylsulfonamido)benzoic acid* was used for further studies.

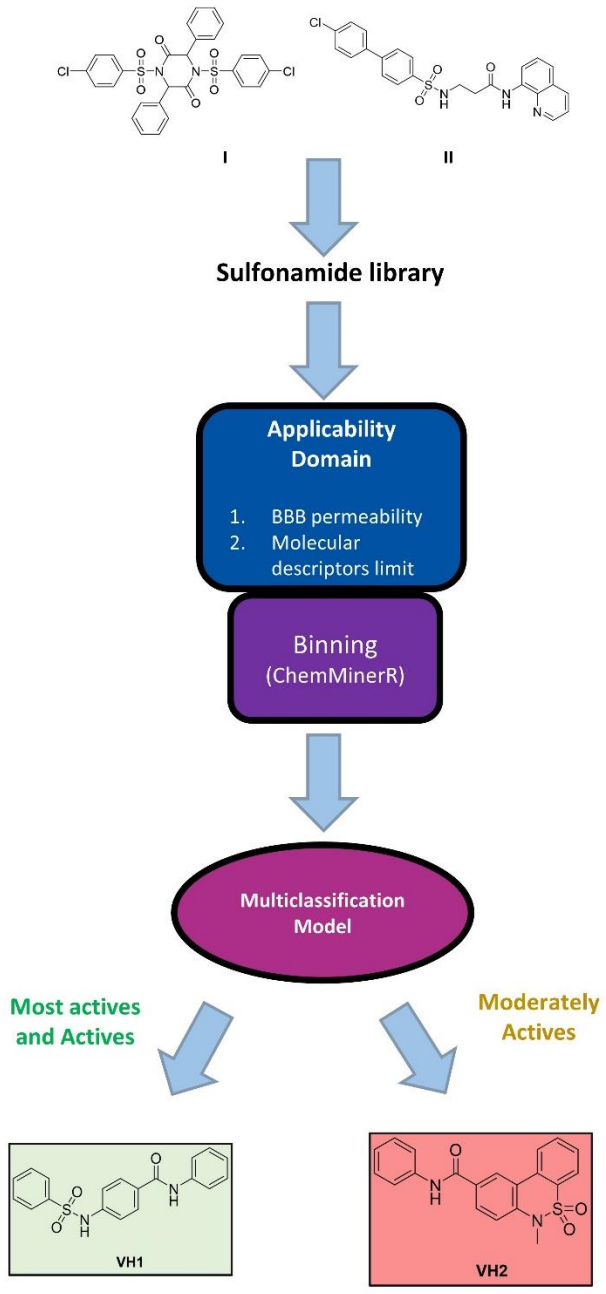

Figure 4.3 Screening of sulfonamide library through the developed ML model to obtain virtual hit.

4.3.2. Chemistry

Step-1: Synthesis of sulfonamide derivative of para-amino benzoic acid

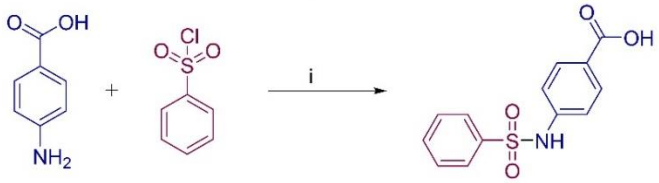

1 2 3

Step-2: Synthesis of derivatives of 4-(phenylsulfonamido)benzoic acid

Scheme 1

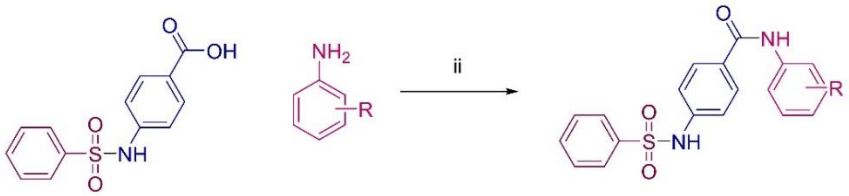

3 4-29 30-55

Comp code	4, 30	5, 31	6, 32	7, 33	8, 34	9, 35	10, 36	11, 37	12, 38	13, 39	14, 40	15, 41	16, 42
R	H	2-F	3-F	4-F	2-Cl	3-Cl	4-Cl	2-Br	3-Br	4-Br	2-OCH_3	3-OCH_3	2-NO_2

Comp code	17, 43	18, 44	19, 45	20, 46	21, 47	22, 48	23, 49	24, 50	25, 51	26, 52	27, 53	28, 54	29, 55
R	3-NO_2	4-NO_2	2-CF_3	3-CF_3	3-$COCH_3$	4-$COCH_3$	2-CH_3	3-CH_3	4-CH_3	2,4-di-CH_3	3,5-di-CH_3	2-C_2H_5	2-NO_2,4-CH_3

Scheme 2

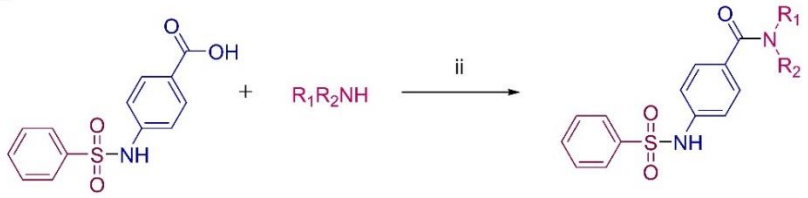

3 56-62 63-69

Comp code	56, 63	57, 64	58, 65	59, 66	60, 67	61, 68	62, 69
R_1	CH_3	C_2H_5	C_4H_9	CH_3	C_2H_5	OH	NH_2
R_2	H	H	H	CH_3	C_2H_5	H	H

Scheme 3

3 70-72 73-75

Comp code	70, 73	71, 74	72, 75
R	CH_3	C_2H_5	C_4H_9

(i) Na_2CO_3, Water:Acetone mixture, rt (ii) TEA, $SOCl_2$, DCM, rt (iii) $SOCl_2$, rt

Figure 4.4 Reaction scheme for synthesis of *4-(phenylsulfonamido)benzoic acid* derivatives.

The synthesis of sulfonamide was initiated by a reaction between the PABA (**2**) and *benzene sulfonyl chloride* (**2**). The lone pair present on the nitrogen atom of PABA initiated a nucleophilic attack on the *sulfonyl* group which resulted in the removal of chlorine and the formation of the sulfonamide bond. The reaction was facilitated in the presence of *sodium carbonate.* The basic pH of the medium helped in the dissolution of PABA, and the removal of the HCl produced during the reaction, which otherwise protonates the amino group of PABA, rendering the nucleophile inactive. The acetone being a polar aprotic solvent did not interfere in the reaction. Further, acetone was added to the reaction mixture to improve the miscibility of oily *benzene sulfonyl chloride* in water and maintain a uniform phase during the reaction. The mixture was concentrated by evaporation of acetone under vacuum, followed by acidification to neutralise the residual *sodium carbonate*. The acid also reacted with the sodium salt of the product and formed precipitate of *4-(phenylsulfonamido) benzoic acid* (**3)**. The trace amount of *benzenesulfonic acid* was formed and remained soluble in an acidic medium due to its lower pka than HCl. It was removed by washing the product with ice-cold water. The dry crude product was recrystallized with ethanol. **Figure 4.4** depicts the synthesis of aromatic amide derivatives (**30 – 55**) from substituted *anilines* (**4 – 29**) in the presence of *triethylamine* and *thionyl chloride*. The yield was obtained between 35 – 85%, with the lowest yield observed among the *ortho* substituents. The polar substituents viz. *nitro*, *methoxy*, *acetyl* displayed lower R_f values. **Scheme 2** represents the synthesis of aliphatic amides and related derivatives (**63 – 69**) with the lowest yield observed for *hydrazide* and *hydroxamate* derivatives. The R_f values of the two derivatives were lowest among all the compounds, with the highest melting points on account of their higher polarity. The synthesis of esters (**73 – 75**) of compound **3** in the presence of *thionyl chloride* and various alcohols (**70 – 72**) is depicted in **Scheme 3**. The yield was high, and their melting points followed the increasing order of molecular mass. Proton NMR data indicated an NH

signal of *sulfonamide* above 10 ppm, with a little deshielding effect among various derivatives (**Scheme 1)**. The position of NH signal of the amide group displayed variation due to alterations of substituents attached to the phenyl ring. It was observed that the *nitro*, *acetyl*, *trifluoromethyl* groups, that have higher negative inductive effect, displayed downfield signals for the NH group. In contrast, the group with higher positive inductive effects such as *methyl*, *methoxy*, present adjacent to phenyl ring, displayed higher shielding. The amides obtained from aliphatic amines displayed higher upfield signals due to the electron releasing effect. Further, the *methoxy* substituent caused higher deshielding of the NH signal than the *acetyl* group due to the direct attachment of an electronegative oxygen atom. The ^{13}C NMR data displayed a carbonyl signal around 165 ppm along with signals from aromatic carbon in the expected region. The mass spectrum of the *chloro* and *bromo* derivatives displayed M^+ and M^{+2} molecular peaks with intensity in a ratio of 3:1 and 1:1, respectively. The IR spectra also indicated the presence of asymmetric and asymmetric stretching of the *sulfonyl* group [212].

4.3.3. *In vitro* cholinesterase inhibitory activity

The study identified compound **30** as a BChE inhibitor through the ML model and displayed IC_{50} value of 503.2 ± 46.917 nM. The ML model also predicted its IC_{50} value in the range of 100 to 1000 nM; hence, the prediction was accurate. Compounds with different substitutions on the phenyl ring associated with the amide bond were synthesised and their IC_{50} values were determined against BChE. Compounds **31**, **34** and **37** having *fluoro*, *chloro* and *bromo* substitutions at *ortho* position resulted in BChE inhibition in a molecular weight dependent manner with IC_{50} values of 140.96 ± 9.625, 61.32 ± 7.21 and 42.64 ± 2.175 nM, respectively (**Table 4.2**). A similar order was also observed in *para*-substituted halogen derivatives, i.e., compound **33** (*p-F*, 689.3 ± 61.159 nM), **36** (*p-Cl*, 272.53 ± 9.803 nM) and **39** (*p-Br*, 183.76 ± 38.675 nM). In contrast, the *meta*-substituted compounds were less potent among the halogen derivatives. They followed a different

trend with *meta-fluoro* derivative (**32,** 922.5 ± 13.376 nM) being the most active followed by *meta-bromo* (**38**, 1816.33 ± 59.599 nM) and *meta-chloro* (**35**, 4557 ± 498.846 nM). Interestingly, the *ortho*-derivatives were found to be 4 to 5 folds more active than *para*-substituted halogen derivatives. In case of *methoxy* derivatives, substitution at *ortho*-position (380.73 ± 41.548 nM) was 7.5-fold more active than *para*-substitution (2817.66 ± 152.15 nM). The *nitro* derivatives showed a different trend with decreasing activity in order of *ortho*, *meta* and *para* substitutions. The *orthro-nitro* derivative (**42**, 113.16 ± 4.179 nM) showed 17- and 62-folds higher activity than *meta-nitro* (**43**, 1936.66 ± 208.959 nM) and *para-nitro* (**44**, 7055.66 ± 520.568 nM) compounds, respectively. The *ortho-trifluoromethyl* substitution showed the lowest inhibitory activity (**45**, 834.9 ± 24.919 nM) among all the substituents at *ortho*-position. In contrast, the *meta-trifluoromethyl* group showed the next most potent compound (**46**, 964.73 ± 82.082 nM) after *meta-fluoro* substitution among all the *meta*-substituents. The *meta-acetyl* substituent (**47**, 1340 ± 143.381 nM) was more potent than *para*-acetyl substituent (**48**, 5800.66 ± 826.489). A similar trend was also observed with *nitro* compounds that have a strong mesomeric effect. Interestingly, *methyl* substitution, an electron releasing group, also showed a trend similar to the electron-withdrawing groups, i.e., *ortho-methyl* substitution (**49**, 67.47 ± 5.116 nM) was found to be most active, followed by *para-methyl* (**51**, 195.46 ± 13.253 nM) and *meta-methyl* (**50**, 2062 ± 125.54 nM) substitutions. Further, the replacement of *methyl* with *ethyl* group (**54**, 46.5 ± 4.773 nM) at *ortho* position resulted in a 1.5-fold more potent BChE inhibitor. The *dimethyl* substitution at the phenyl ring provided some important observations, indicating the importance of *ortho*- and *para*-positions for the BChE inhibitory activity. 2, 4-di-*methyl* substitution (**52**, 40.59 ± 0.89 nM) was 22 folds more potent than 3, 5 di-*methyl* substitution (**53**, 898.9 ± 29.572 nM). Further, *2, 4-di-methyl* substitution was 1.5 folds more active than *ortho-monomethyl* substitution. However, the replacement of *ortho-methyl* with the *nitro* group in compound

52 resulted in *ortho-nitro, para-methyl* derivative (**55**, 450.4 ± 20.603 nM) that displayed lower activity.

The compounds obtained from **Schemes 2** and **3** were evaluated for BChE inhibition at 50 μM. It was found that the compounds have lower potency than the aromatic derivatives. Further, some of the compounds displayed precipitation in assay medium at 100 μM that interfered with absorbance signals. Hence, the IC_{50} of these compounds were not determined. However, the data displayed that the aromatic amide substitutions were responsible for BChE inhibition and the replacement with aliphatic amides and esters resulted in the loss of activity. Replacement of OH in compound **3** (16.42 % ± 1.04) with *methyl* ester (**73**, 4.35 % ± 0.55) and *N-methyl* amide (**63**, 11.14 % ± 1.36) resulted in a decrease in the activity. In the case of amide derivatives, it was observed that an increase in the size of the aliphatic chain viz., *ethyl* (**64**, 14.03% ± 0.85) and *butyl* (**65**, 32.14 % ± 3.18), resulted in higher BChE inhibition. A similar trend was observed with ester derivatives, i.e., *ethyl* (74, 15.95 % ± 0.28) and *butyl* (46.53 % ± 0.2). Further, the *dimethyl amide* (**66**, 13.57 % ± 3.97) and *diethyl amide* (**67**, 17.14 % ± 1.58) also showed BChE inhibition similar to the amides of corresponding monoamine derivatives (**Table 4.3**). Finally, the carboxylic acid group of compound **3** was replaced with the polar groups viz. *hydroxamic acid* (**68**, 20.03 % ± 1.42) and *hydrazide* (**69**, 17.83 % ± 0.37), which resulted in almost similar inhibitions. The IC_{50} and % inhibition data showed that the *ortho*-position of the *phenyl* ring that is linked through amide bond is dominant and affects the potency of the inhibitors positively.

AChE shares a structural similarity with BChE and usually, an inhibitor inhibits AChE and BChE both. The synthesised compounds displayed a low % inhibition of AChE at 50 μM concentration. The % inhibition data indicated that eighteen compounds of **Scheme 1** had AChE inhibition below 10 %.

Table 4.2 Inhibitory potencies of *4-(phenylsulfonamido) benzoic acid* derivatives (**30 – 55**) against cholinesterase enzymes.

Compound code	BChE IC_{50} (nM) *	AChE (% inhibition) *
30	503.2 ± 46.917	10.32 % ± 0.72
31	140.96 ± 9.265	0.13 % ± 2.89
32	922.5 ± 13.376	na
33	689.3 ± 61.159	0.62 % ± 1.94
34	**61.32 ± 7.21**	**1.98 % ± 2.02**
35	4557 ± 498.846	6.27 % ± 4.3
36	272.53 ± 9.803	8.44 % ± 2.25
37	**42.64 ± 2.175**	**na**
38	1816.33 ± 59.599	19.18 % ± 3.62
39	183.76 ± 38.675	5.07 % ± 1.28
40	380.73 ± 41.548	1.64 % ± 3.63
41	2817.66 ± 152.15	0.35 % ± 2.04
42	113.16 ± 4.179	9.16 % ± 2.28
43	1936.66 ± 208.959	2.12 % ± 1.85
44	7055.66 ± 520.568	7.52 % ± 2.64
45	834.9 ± 24.919	16.52 % ± 5.39
46	964.73 ± 82.082	10.4 % ± 1.11
47	1340 ± 143.381	na
48	5800.66 ± 826.489	3.32 % ± 0.21
49	67.47 ± 5.116	11.2 % ± 0.94
50	2062 ± 125.54	0.35 % ± 1.37
51	195.46 ± 13.253	2.67 % ± 6.38
52	40.59 ± 0.89	10.93 % ± 7.87
53	898.9 ± 29.572	23.5 % ± 2.64
54	**46.5 ± 4.773**	**0.52 % ± 1.42**
55	450.4 ± 20.603	11.01 % ± 3.63
Donepezil	2677.33 ± 8.75	94.65% ± 1.14

* Data expressed as Mean ± SEM, na – not active.

Table 4.3 Inhibition of *4-(phenylsulfonamido) benzoic acid* derivatives (**3**, **63** – **69**, **73** – **75**) against cholinesterase enzymes.

Compound code	BChE (% inhibition) *	AChE (% inhibition) *
3	16.42% ± 1.04	94.65 % ± 1.14
63	11.14 ± 1.36	9.18 ± 6.06
64	14.03 ± 0.85	14.56 ± 0.68
65	32.14 ± 3.18	14.73 ± 1.23
66	13.57 ± 3.97	13.26 ± 3.46
67	17.14 ± 1.58	12.47 ± 2.3
68	20.03 ± 1.42	18.26 ± 1.58
69	17.83 ± 0.37	17.37 ± 0.73
73	4.35 ± 0.55	14.19 ± 1.38
74	15.95 ± 0.28	10.82 ± 0.94
75	46.53 ± 0.2	13.13 ± 0.93

* Data expressed as Mean ± SEM.

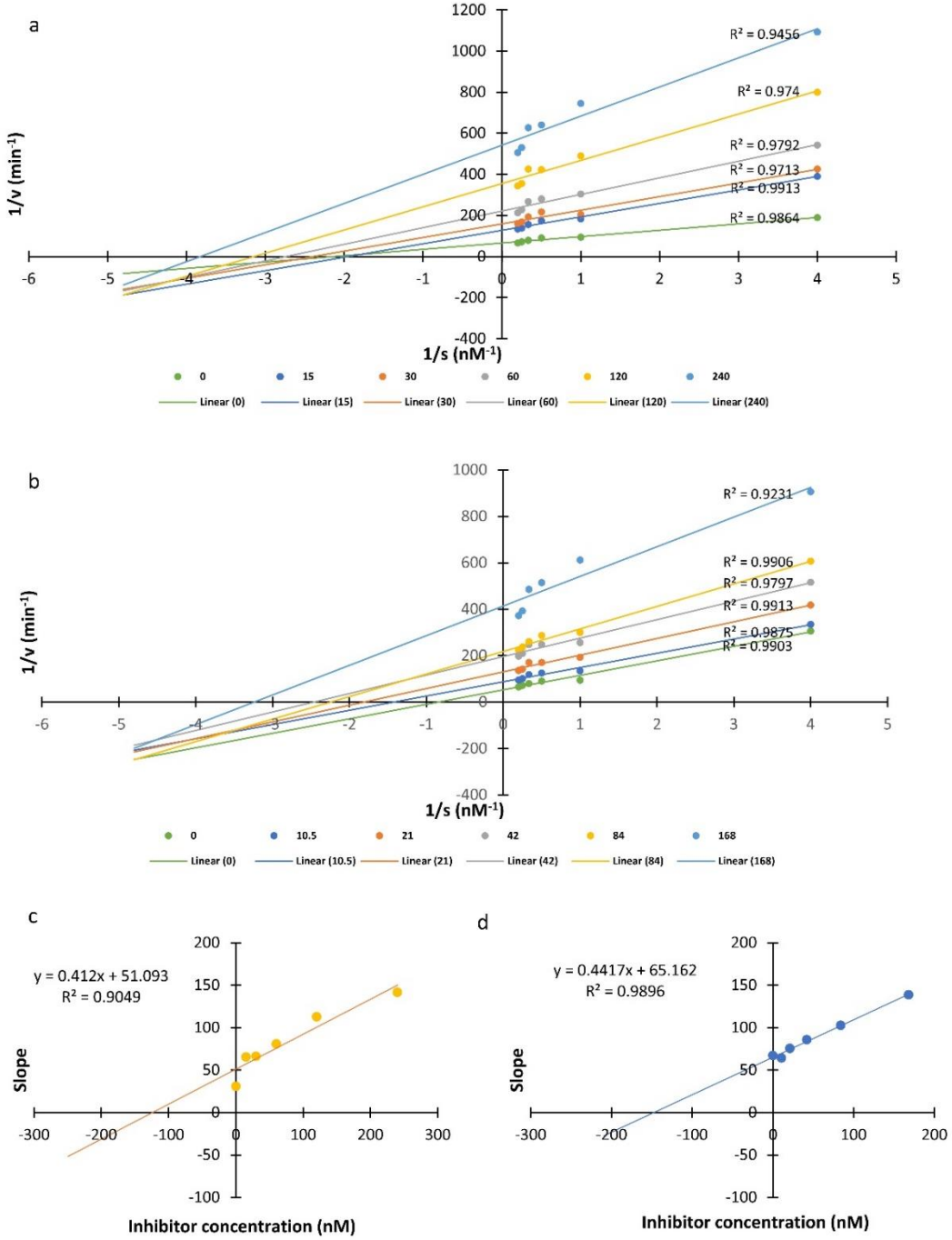

Figure 4.5 Lineweaver Burk double reciprocal plot of compounds (a) **34** and (b) **37**. Dixon plot of compound (c) **34** and (d) **37** for Ki calculation.

The *meta-bromo* (**38**, 19.18 % ± 3.62), *ortho-trifluoromethyl* (**45**, 16.52 % ± 5.39), *meta-trifluoromethyl* (**46**, 10.4 % ± 1.11), *ortho-methyl* (**49**, 11.2 % ± 0.94), *ortho-para-dimethyl* (**52**, 10.93 % ± 7.87), *meta-dimethyl* (53, 23.5 % ± 2.64) and *ortho-nitro, para-methyl* (**55**, 11.01 % ± 3.63) substitutions on the *phenyl* ring bonded through amide bond

displayed more than 10% inhibition. In case of **Schemes 2** and **3**, all the substituents except the *hydrazide* displayed AChE inhibition above 10 % at 50 μM. The carboxylic acid intermediate (**3**) had higher inhibition than most aliphatic derivatives. The results indicated that the synthesised compounds have only a low AChE inhibition and confer a higher BChE selectivity. Compounds **34**, **37** and **54** showed good IC_{50} values against BChE and almost no inhibition of AChE, conferring them the most selective BChE inhibitors and were used in further studies.

The double reciprocal Lineweaver Burk plot suggested that compounds **34** and **37** have a mixed-type inhibition of BChE inhibition. The intersecting lines converged in the third quadrant of the plot, indicating that the inhibitors have a higher affinity toward enzyme-substrate complex ($\alpha < 1$) rather than free enzyme (**Figure 4.5**). Further, the Dixon plots were used to determine the inhibition constant (Ki). The inhibition constant for compounds **34** and **37** were found to be 124.01 and 147.52 nM, respectively (**Figure 4.5**).

4.3.4. Cell Viability (MTT Assay)

The cell viability was found to be 59.82 % ± 3.37, 61.17 % ± 1.96 and 57.78 % ± 2.03 for compounds **34**, **37** and **54,** respectively, at 100 μM concentration. There was a dose-dependent reduction in cell viability on treatment with the compounds. Significant toxicity for compounds **34** and **37** was observed at 1190- and 819-folds higher concentrations, respectively, than the IC_{50} values against BChE of the compounds (**Figure 4.6**).

4.3.5. *In vitro* blood-brain barrier permeation assay

The BBB permeability is critical for a compound targeting the brain [147]. A set of nine commercially available compounds were used to establish the correlation in the study [190, 211]. The permeability (Pe) values of the selected compounds were determined and are listed in **Table 4.4**. The compounds were found to be BBB permeable, with halogen derivatives being more permeable.

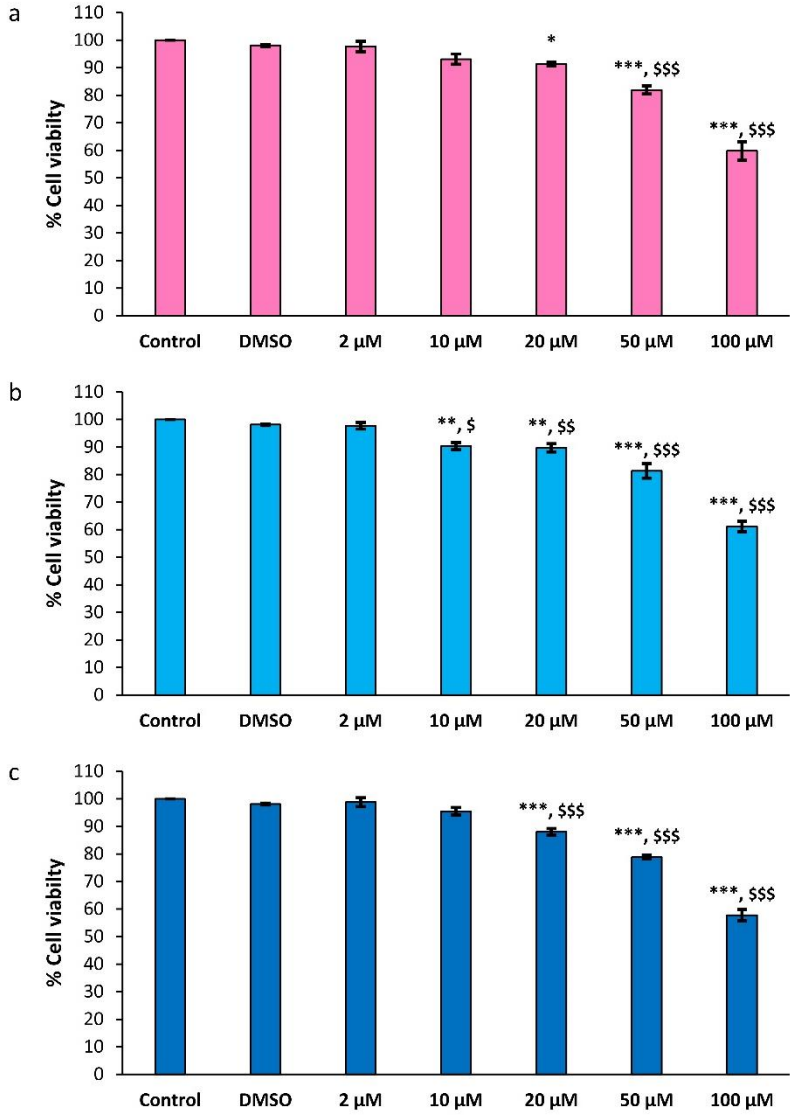

Figure 4.6 Cell viability assay of compounds (a) **34** (b) **37** and (c) **54** on SH-SY5Y cells. PBS was taken as control and data are expressed as Mean ± SD. One-way ANOVA was applied followed by Newman-Keuls multiple comparison test to compare all column pairs ($^{*}p < 0.05$ compared to control; $^{**}p < 0.01$ compared to control, $^{***}p < 0.001$ compared to control, $^{\$\$}p < 0.01$ compared to to DMSO; $^{\$\$\$}p < 0.001$ compared to DMSO).

Table 4.4 Permeability data for selected compounds obtained from PAMPA-BBB assay.

Compound code	Pe (10^{-6} cm s^{-1})
34	7.394 ± 0.546
37	7.017 ± 0.243
54	6.968 ± 0.273

All data were expressed as Mean ± SD for experiment performed in triplicates.
Compounds with Pe > 4.324×10^{-6} cm s^{-1} could cross the BBB (CNS+), Pe < 1.846×10^{-6} cm s^{-1} could not cross the BBB (CNS−) and 1.846×10^{-6} cm s^{-1} < Pe < 4.324×10^{-6} cm s^{-1} showed uncertain BBB permeation (CNS ±).

4.3.6. *In silico* ADMET and molecular property analysis

The Lipinski's rule of five (RO5) is a group of important molecular properties predictors of drug-likeness. The Pan-assay interference compounds (PAINS) are a group of functional groups and substructures that may interfere with the bioanalytical process or react with proteins through autoxidation, cystine oxidation, membrane disruption, aggregation, and chelation. It was observed that all the compounds showed no violation of RO5 and did not have any PAINS functional group. The partition coefficient (logP) is another important property for CNS permeability. It was found that with the increase in molecular weight of the halogen derivatives (**31** – **40**), the LogP of the compounds increased. The alkyl substituents on the aromatic ring (**49 – 55**) render them higher lipophilicity, and in the contrary, the *nitro* (**42 – 44**) and *methoxy* (**40 – 41**) substituents decrease the logP. In the case of the aliphatic amide substituents (**63 – 68**), a substantial decrease in the logP was observed and a higher logP were reported for ester derivatives (**73 – 75**) of compound **3**. The intestinal absorption of the synthesized compounds was found to be reasonable, i.e., above 85 %, except hydroxamate and hydrazide derivatives. The predicted CNS permeability was found to be good for compounds **34, 35, 37, 38, 39, 45, 46, 51, 52, 53** and optimal permeability was observed for the remaining compounds. CYP2D6 and CYP3A4 are responsible for the metabolism of donepezil. Enzyme CYP2D6 is responsible for hydroxylation, deamination and dealkylation, while CYP3A4 leads to the oxidation of aromatic rings, aldehydes and heteroatoms, hydroxylation, olefinic epoxidation, N- and O- dealkylation [213, 214]. It was predicted that all the compounds in the series were substrates for CYP3A4 and not for CYP2D6. Further, the compounds were non-inhibitors for the Human ether-à-go-go related gene (hERG) 1 channel, which regulates the plateau phase of the cardiac cycle (**Table 4.5**).

Table 4.5 Molecular and selected ADME properties of synthesised compounds.

Compound code	LogP	Intestinal absorption (%)	CNS permeability	CYP2D6 substrate	CYP3A4 substrate	CYP2D6 inhibitior	CYP3A4 inhibitior	hERG I inhibitor
3	2.185	99.154	-2.444	No	No	No	No	No
30	3.739	91.383	-2.063	No	Yes	No	Yes	No
31	3.878	90.576	-2.1	No	Yes	No	Yes	No
32	3.878	91.427	-2.099	No	Yes	No	Yes	No
33	3.878	92.319	-2.183	No	Yes	No	Yes	No
34	4.393	89.611	-1.948	No	Yes	No	Yes	No
35	4.393	90.546	-1.943	No	Yes	No	Yes	No
36	4.393	91.363	-2.02	No	Yes	No	Yes	No
37	4.502	89.544	-1.926	No	Yes	No	Yes	No
38	4.502	90.479	-1.92	No	Yes	No	Yes	No
39	4.502	91.296	-1.998	No	Yes	No	Yes	No
40	3.748	91.304	-2.225	No	Yes	No	Yes	No
41	3.445	86.465	-2.241	No	Yes	No	Yes	No
42	3.647	87.973	-2.281	No	Yes	No	Yes	No
43	3.647	91.439	-2.272	No	Yes	No	Yes	No
44	3.647	91.456	-2.283	No	Yes	No	Yes	No
45	4.758	90.674	-1.972	No	Yes	No	Yes	No
46	4.758	88.987	-1.899	No	Yes	No	Yes	No
47	3.942	96.223	-2.202	No	Yes	No	Yes	No
48	3.942	91.019	-2.193	No	Yes	No	Yes	No
49	4.048	93.233	-2.053	No	Yes	No	Yes	No
50	4.048	93.28	-2.062	No	Yes	No	Yes	No
51	4.048	91.413	-1.987	No	Yes	No	Yes	No
52	4.356	92.804	-1.978	No	Yes	No	Yes	No
53	4.356	93.31	-1.989	No	Yes	No	Yes	No
54	4.302	93.013	-2.095	No	Yes	No	Yes	No
55	3.956	87.499	-2.28	No	Yes	No	Yes	No
63	1.847	91.375	-2.473	No	Yes	No	No	No
64	2.237	90.956	-2.481	No	Yes	No	No	No
65	3.017	90.814	-2.496	No	Yes	No	No	No
66	2.189	91.165	-2.384	No	Yes	No	No	No
67	2.969	90.327	-2.4	No	Yes	No	No	No
68	1.606	70.739	-2.708	No	Yes	No	No	No
69	1.090	72.462	-2.797	No	Yes	No	No	No
73	2.274	93.098	-2.364	No	Yes	No	No	No
74	2.664	92.679	-2.372	No	Yes	No	No	No
75	3.444	92.806	-2.391	No	Yes	No	Yes	No
Donepezil	4.361	92.731	-1.437	Yes	Yes	Yes	Yes	No

CNS permeability – LogPS > -2 : CNS permeable and LogPS < -3 CNS impermeable.

4.3.7. Molecular docking

The comparison of protein-ligand interactions and the superimposition of the docking pose revealed various crucial information (**Figures 4.7 and 4.8**). It was observed that the binding site of *fluoro* derivatives (**31**, **32** and **33**) and compound **30** on the protein overlapped. The π-π and π-alkyl interactions with Tyr332 and Leu285, respectively, stabilised the central phenyl ring in compound **31** and was absent in compound **33**, also

reflected in IC_{50}(s). The docking pose of *para-chloro* derivative (**36**) displayed a much higher deviation from compound **30** as well as the other two *chloro* derivatives (**34** and **35**). Compound **35** had a similar interaction profile as of **30,** along with two additional halogen interactions. Compound **34** displayed more interactions with the enzyme, which was indicated by a lower IC_{50} value. In case of the *bromo* compounds, it was observed that compound **37** displayed more interactions with a low IC_{50} value. Phe329 and His438 displayed halogen bonds with the *ortho-bromo* group while the *meta* (**38**) and *para* (**39**) substituted bromine produced a single halogen bond with Asp283 and Ser287, respectively. Compound **39** displayed higher interaction than **38**.

The *meta-methoxy* (**40**) derivative was well placed in the cavity, similar to compound **30** with an additional hydrogen bonding between *methoxy* group and His438 residue. This resulted in lower IC_{50} value of the compound than **30**. On the other hand, the *para*-substitution resulted in the positioning of *para-methoxy phenyl* ring at the entrance of the cavity and the *methoxy* group formed hydrogen bond with Asp283 and Asn289. The *nitro* substituted compounds depicted a trend similar to their corresponding IC_{50} values. It was observed that the *ortho*-substituted compound **42** produced most interactions while *para*-substitution (**44**) had least interactions. The *tri-fluoro methyl* group of compounds (**45** and **46**) helped in halogen bond formation with residue located near the acyl binding pocket. Interestingly, both compounds have an RMS deviation of 1.32 Å with each other and different interaction patterns, but they had comparable IC_{50} values. The *meta-acetyl* substituted compound **47** displayed an unfavourable interaction with Leu285 residue. The *para-acetyl* derivative (**48**) displayed interactions only with oxyanion hole and acyl binding pocket and missing interaction with other major sites. Hence, higher IC_{50} values were observed for both these compounds.

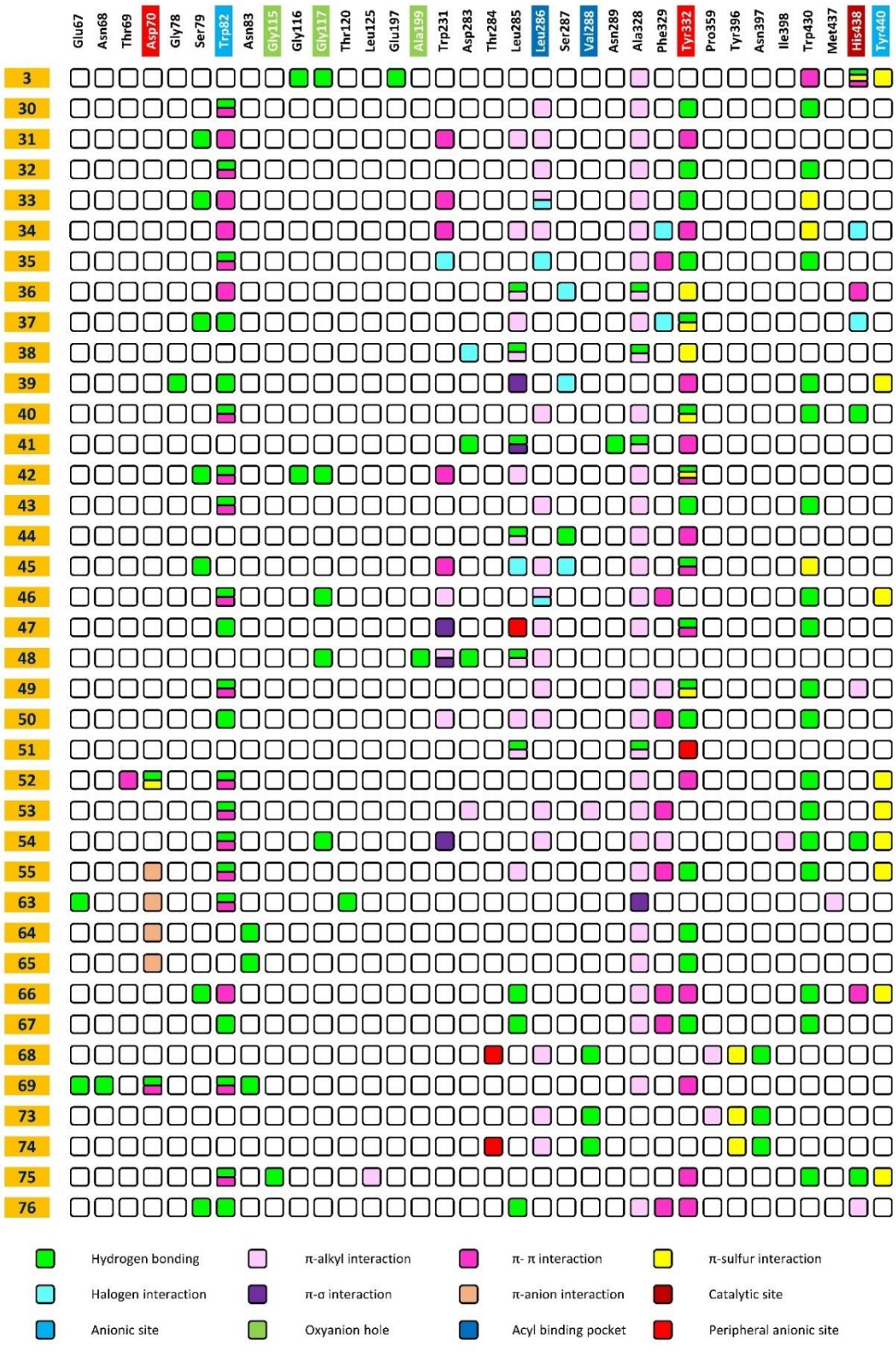

Figure 4.7 Protein-ligand interaction profile of the compounds obtained from molecular docking.

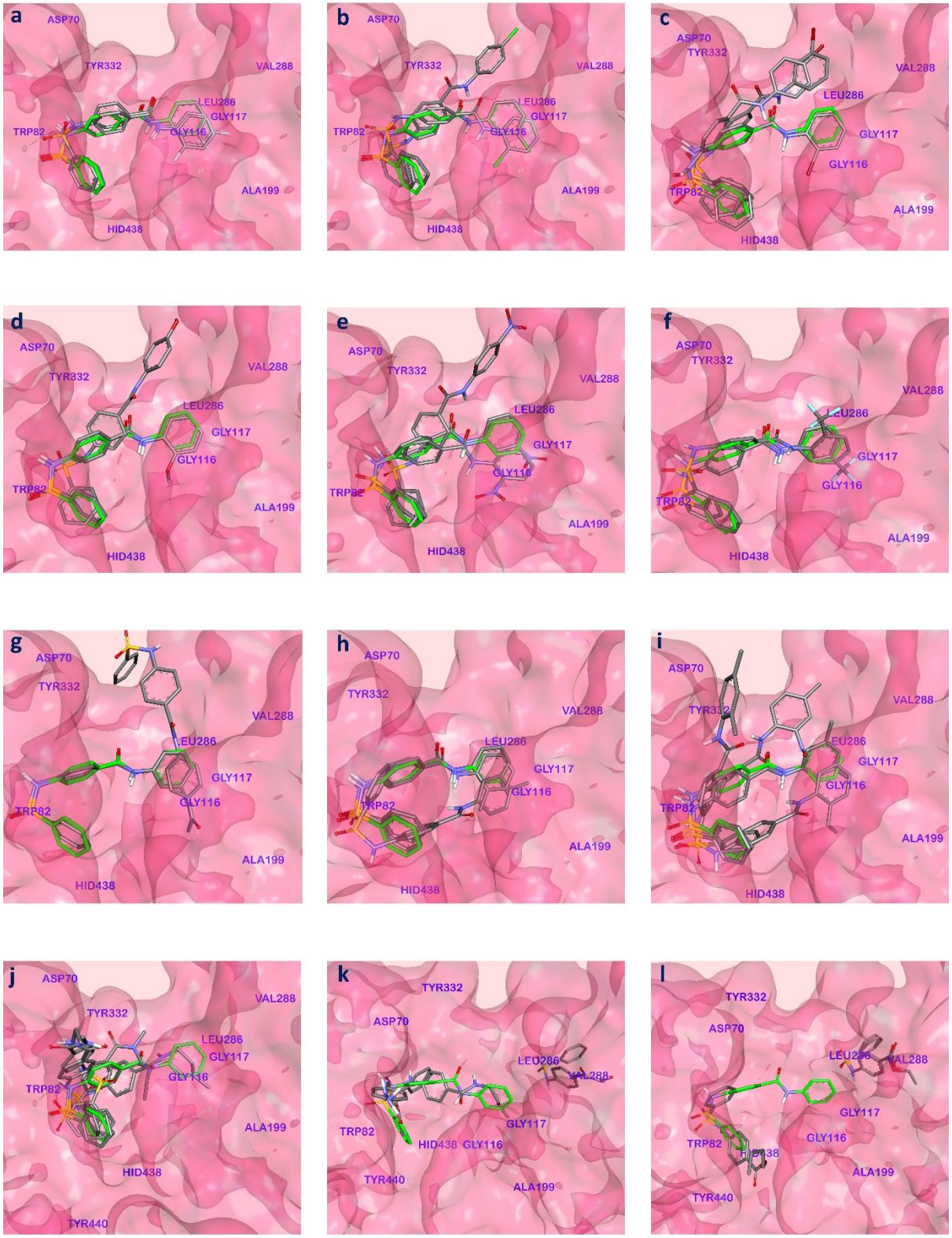

Figure 4.8 Orientation of the docking poses in the cavity of BChE enzyme.
(a) *fluoro*, (b) *chloro*, (c) *bromo*, (d) *methoxy*, (e) *nitro*, (f) *trifluoro-methyl*, (g) *acetyl*, (h) *methyl*, (i) di-substituted and *ethyl*, (j) alkyl amides, (k) esters and (l) hydrazide and hydroxamate derivatives superimposed on prototype compound **30** (in green).

The *methyl* substituted compounds (**49**, **50** and **51**) displayed good interactions with BChE. However, the IC_{50} value of the compound **50** was higher, which may due to the

weaker alkyl interactions of the *methyl* group and its presence in the solvent-exposed region. The *dialkyl*-substituted derivatives (**52**, **53** and **55**) displayed strong interaction with the enzyme, also indicated in their IC_{50} values. The *ortho-ethyl* substituted derivative was bound deep inside the cavity and interacted with all major sites of the enzyme and hence, displayed the lowest IC_{50}.

Further, the aliphatic amide derivative displayed interesting docking results. It was observed that the n-*butyl* chain (**65**) was buried deep in the acyl binding site, while the corresponding mono-*methyl* and *ethyl* chains (**63** and **64**) were located near PAS owing to the hydrophobicity. Further, the *dimethyl* and *diethyl* derivatives (**66** and **67**) were located deeper in the cavity than the corresponding mono-alkyl derivatives. The *hydroxamate* derivative (**68**) interacted with the acyl binding pocket, while the *hydrazide* derivative (**69**) interacted with the anionic site and PAS. Similarly, the *methyl* and *ethyl* esters (**73** and **74**) also interacted with the acyl binding pocket, while butyl ester derivative (**75**) was buried deep inside and interacted with the active site, anionic site and PAS.

4.3.8. Quantitative structure-activity relationship

In the present work, two QSAR models were developed on different sets of descriptors Compounds **30** – **55** were used for QSAR studies due to the availability of their IC_{50} values.

4.3.8.1. 2-dimensional descriptors based QSAR

The two-dimensional descriptors obtained from the Mordred server were subjected to a correlation filter with a cut-off value of 0.9 and zero variance filter to obtain 263 descriptors. The sequential feature selectors further reduced the count to fifteen features with the help of a linear regression algorithm. It was observed that a combination of five and more features resulted in good performance of the training set, as indicated in **Figure 4.9(a)**. Hence, various combinations of 5 – 12 features were generated for training QSAR

models using the decision tree regression algorithm. The r^2 of the training set was found to be 1 with zero mean absolute error (MAE) and mean squared error (MSE) of the selected model. The internal validation, using the leave one out (LOO) method, indicated Q^2 and mean r^2_m (LOO) to be 1 each with $\Delta\ r^2_m$ (LOO) value 0 for the final models. Further, the selected model has highest Q^2_{F1} (0.968) and Q^2_{F2} (0.963) values with r^2_m and $\Delta\ r^2_m$ values satisfying the criteria for good models ($r^2_m > 0.5$ and $\Delta\ r^2_m < 0.2$) on the test set (**Table 4.6**). The feature importance of the decision tree model is presented in the **Figure 4.9(b)** and decision tree is represented in **Figure S1 in appendix**.

The JGI7 descriptor has the highest importance (63.33 %). It is the mean topological charge index of 7th order that evaluates the charge transfer between the atom pairs. Lower value of JGI7 was favourable for BChE inhibition, as indicated in **Figure 9(c)**. It was found that *ortho*-substituted compounds **34**, **37** and **49** have low JGI7 values with good BChE inhibition, i.e., higher pIC_{50}. While compounds **44** and **48** have higher JGI7 values with moderate inhibition. The second important descriptor was GATS5Z, with an importance coefficient of 15.63 %. GATS are a group of Geary coefficients that indicates the spatial autocorrelation of molecular property among the constituent atoms of a molecule based on the topological distance. A value between 0 – 1, 1 and > 1 indicates positive, no and negative correlation among the atoms, respectively. GATS5Z represents the Geary coefficient of lag 5 weighted by atomic number. The lower value of GATS5Z is favourable and correspond to lower IC_{50} or higher pIC_{50} value of compounds **34** and **37**. In case of GATS7P, that describes the polarizability, it was observed that lower value leads to a decrease in enzyme inhibition activity as observed with compounds **35**, **38**, **47** and **50**. On the other hand, the increased value of GATS7P led to lower IC_{50} values, as in the case of compounds **49** and **52**. GATS8d is the Geary coefficient of lag 8 weighted by sigma electrons that represent the electronic environment related to sigma bonds in the

molecule. It was observed that a lower GATS8d value resulted in better inhibition which was observed in case of the *ortho*-substituents. GATS6i represents the ionisation potential of the Geary coefficient. It was observed that its lower values resulted in lower IC_{50} or higher pIC_{50}. GATS2v and SM1_DzZ are the remaining descriptors of the model that were not able to differentiate among compounds with similar functional groups.

4.3.8.2. Pharmacophore based QSAR

The second QSAR model was developed from CATS based topological atom-pair descriptors, that represent potential pharmacophore points [215]. The application of correlation (cut-off > 0.9) and zero variance filters resulted in the selection of 25 features. A set of 15 features were subsequently selected by employing using sequential feature selection. It was observed that a combination of 9 or more features was optimum for model development, as indicated in the **Figure 4.9(d)**. Hence, all possible combinations of 9 -14 descriptors were employed using linear regression. The models that displayed r^2 more than 0.9 with a low MSE value were selected and subjected to internal validation using LOO and external validation on a separate test set. The selected model showed r^2 0.924, Q^2_{LOO}, mean $r^2_{m\ (LOO)}$, $\Delta r^2_{m\ (LOO)}$ of 0.934, 0.923, 0.904 ± 0.013 and 0.063 ± 0.009, respectively (**Table 4.6**).

The performance of the test set was good with Q^2_{F1} and Q^2_{F2} values of 0.951 and 0.942, respectively. r^2_m and Δr^2_m values in the test set were 0.923 and 0.027, respectively, which were far better than the acceptable limits. Overall, the quality of the developed model was good and represented in the form of linear equation 1.

pIC_{50} = 6.318 - 0.163 * CATS_AA5 - 0.084 * CATS_AA8 - 0.356 * CATS_AL2 - 0.246 * CATS_AL5 + 0.472 * CATS_AL6 + 0.173 * CATS_AN7 + 0.236 * CATS_LL1 + 0.632 * CATS_LL3 + 0.524 * CATS_LL5 - 1.674 * CATS_LL6 + 1.441 * CATS_LL7 - 1.037 * CATS_LL8 (**1**)

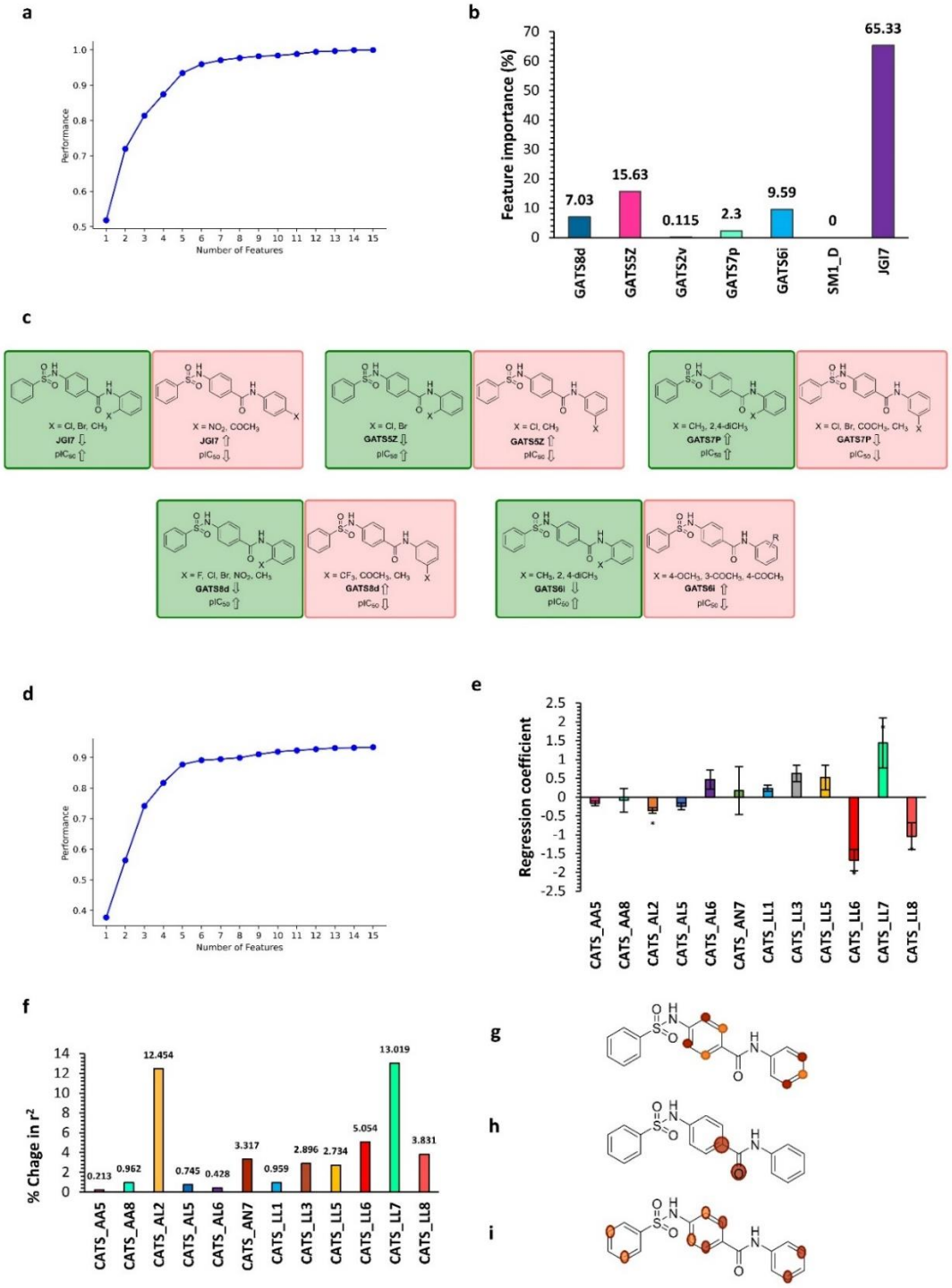

Figure 4.9 Results of the developed QSAR models.
(a) Identification of optimum number of features for decision tree QSAR models. (b) Feature importance of descriptors of decision tree QSAR model. (c) Trends of biological activity of individual descriptor used for development of decision tree QSAR. (d) Identification of optimum number of features for regression based QSAR model. (e) Regression coefficient of QSAR equation developed from CATS2D descriptors ($^{*}p < 0.05$ compared constant obtained from regression equation). (f) % change in r^2 representing feature importance of the selected descriptors for regression based QSAR model. (g, h, i) Representation of CATS_LL7, CAT_AL2 and CATS_LL6 features, respectively

Table 4.6 Performance of the final QSAR models.

Algorithm	**Decision tree regression**	**Linear regression**	**Linear regression**
Descriptors	GATS8d, GATS5Z, GATS2v, GATS7p, GATS6i, SM1_D, JGI7	CATS_AA5, CATS_AA8, CATS_AL2, CATS_AL5, CATS_AL6, CATS_AN7, CATS_LL1, CATS_LL3, CATS_LL5, CATS_LL6, CATS_LL7, CATS_LL8	CATS_AL2, CATS_LL6, CATS_LL7
r^2	1	0.934	0.522
MSE	0	0.028	0.246
Q^2(LOO)	1.0 ± 0.0	0.923 ± 0.0	0.518 ± 0.0
MAE(LOO)	0.0 ± 0.0	0.027 ± 0.003	0.244 ± 0.019
MSE(LOO)	0.0 ± 0.0	0.107 ± 0.006	0.393 ± 0.021
mean r^2m (LOO)	1.0 ± 0.0	0.904 ± 0.013	0.354 ± 0.048
Δ r^2m (LOO)	0.0 ± 0.0	0.063 ± 0.009	0.341 ± 0.017
Q^2_{F1}	0.968	0.951	-4.883
Q^2_{F2}	0.963	0.942	-7.951
MAE (test)	0.122	0.934	0.441
MSE (test)	0.02	0.028	0.475
r^2m (test)	0.948	0.923 ± 0.0	-7.951
Δ r^2m (test)	0.03	0.027 ± 0.003	0

It was observed that CATS_LL7 was the most important feature due to a 13.019 % drop in r^2 value, after its removal from the model (**Figure 4.9(f)**). CATS_LL7 indicated that the two lipophilic groups were separated by 7 atoms (**Figure 4.9g**). An increase in CATS_LL7 value led to the increase in pIC_{50} and BChE inhibition, indicated by a positive correlation in the regression coefficient plot (**Figure 4.9(e)**). The substitution at *ortho*-position resulted in higher CATS_LL7 value viz compounds **34**, **37**, **49**, **52** and **54**. While compounds **41**, **42** and **44** displayed the lowest value for the descriptor, that led to a decrease in pIC_{50} or increase in IC_{50} values. The second most important feature was CATS_AL2, which indicated a hydrogen bond acceptor separated from the lipophilic group through 2 atoms (**Figure 4.9(h)**). An increase in the descriptor value resulted in a decrease in pIC_{50}, i.e., poor inhibition. Compounds **41**, **43**, **44** and **48** displayed lower pIC_{50} with an increase in CATS_AL2 values. CATS_LL6 is the third essential feature that is negatively correlated with the pIC_{50} value (**Figure 4.9(i)**). The three features were

statistically significant and hence provided a clear trend. The other features viz. CATS_AA5, CATS_AA8, CATS_AL5, CATS_AL6, CATS_AN7, CATS_LL1, CATS_LL3, CATS_LL5 and CATS_LL8 were important, but their regression coefficients were not statistically significant with respect to the intercept of the QSAR equation and could not be used for prediction of any individual trend. However, these features did contribute to the performance of the QSAR model. The model developed with only three selected significant descriptors i.e., CATS_AL2, CATS_LL6 and CATS_LL7, had poor performance, as indicated in **Table 4.6**.

4.3.9. Molecular dynamics

MD was carried out using AMBER 20 for compounds **34**, **37** and donepezil. The energy minimisation of the BChE and complexes with compounds **34**, **37** and donepezil resulted in a reduction in the potential energies from -194630, -194670, -194700 and -194390 to -298650, -298830, -298820 and -298580 Kcal/mol, respectively. The minimisation involved a steady reduction in energy through the application of weight restrain over the protein, which resulted in stable complexes (**Table T1 in appendix**). It was followed by heating the systems from 150 to 310.15 K through the application of Andersen-like temperature coupling scheme. The desired temperature of the complexes was achieved with 5 - 6 ps of run and was almost held constant for the rest of the time. The mean temperatures of BChE and BChE complexed with compounds **34**, **37** and donepezil were 310.08 ± 1.162, 310.52 ± 1.144, 310.01 ± 1.145 and 310.41 ± 1.079 K, respectively. It was followed by density equilibration of the systems in order to provide stabilisation during the MD. The BChE and BChE complexed with compounds **34**, **37** and donepezil attained a unit density at 51, 43, 44, and 47 ps, respectively. After attaining the unit density, the mean density of all systems was found to be 1.011 ± 0.03 g/cm^3. This was followed by pre-MD equilibration to achieve stable complexes before a prolonged run. The mean Root Mean Square Deviation (RMSD) of BChE and BChE complexed with

compounds **34**, **37** and donepezil were 1.005 ± 0.138, 1.121 ± 0.149, 1.027 ± 0.123 and 0.973 ± 0.097 Å, respectively, for a period of 1 ns (**Figure S2 – S5 in appendix**).

The MD run was performed for 50 ns and trajectories obtained were further analysed. The RMSD was calculated using the first frame as a reference for protein backbone and smaller values indicated stable complex. A globular protein usually has RMSD in the range of 1 – 3 Å. The mean RMSD value was found to be 1.283 ± 0.153, 1.226 ± 0.109, 1.325 ± 0.141 and 1.544 ± 0.175 Å, for BChE and BChE complexed with compounds **34**, **37** and donepezil, respectively. However, it was found that the average RMSD of compounds **34** and **37** were 1.198 ± 0.067 and 1.320 ± 0.1 Å, respectively, for the last 20 ns of simulation, which was lower than the protein, i.e., 1.360 ± 0.096 Å. Further, all the complexes appeared stable during the simulation. The ligand RMSD displayed a similar trend for compounds **34**, **37** and donepezil with mean RMSD of 1.460 ± 0.284, 1.271 ± 0.387 and 1.198 ± 0.328 Å, respectively. The root mean square fluctuation (RMSF) indicated the flexibility and fluctuations in the residues of the protein. The protein and protein-ligand complexes did not show a significant change in RMSF, indicating protein stability. Compound **34** stabilised Ser79, Trp82, Leu285, Leu286 and Tyr332 residues, while compound **37** stabilised Trp82, Leu285, Tyr332 and His438. Further, donepezil interacted with residues of PAS as well as anionic site (Asp78 – Asn83), but displayed no stable interactions with acyl binding pocket, which was reflected in RMSF data. It was evident from the ligand RMSF data that both compounds **34** and **37** displayed low fluctuations in the halogen bearing *phenyl* ring, which reflected the strength of the halogen bond with protein. On the other hand, the *sulfonyl* bearing *phenyl* group, which is exposed to the exterior environment, showed a higher deviation for compound **37**. In case of donepezil, it was observed that *N-benzyl* moiety showed maximum deviation, as it did not display any interaction with the protein in docking studies. The 4^{th} – 6^{th} atoms of the

aromatic ring displayed minimum RMSF, which was apparently due to π-interactions with Ala328, Phe329 and Tyr332 (**Figure 4.10**). Solvent accessible surface area (SASA) is a measure of solvent-protein interaction. The mean SASA for BChE and BChE complexes with compounds **34**, **37** and donepezil were 21114 ± 374.686, 21216.4 ± 415.306, 21187.6 ± 348.084 and 21453.7 ± 427.358 $Å^2$, respectively. It was found that the ligand-binding led to an increase in SASA of protein. The increase in SASA was more significant for donepezil followed by compounds **34** and **37**. The docking pose of donepezil indicated that the methoxy groups were solvent exposed, which would be responsible for increased SASA. In the case of SASA of ligands, the mean SASA of compound **37** and donepezil was 112.35 ± 24.356 and 110.72 ± 29.722 $Å^2$, respectively, which was higher than the mean SASA of 85.16 ± 20.116 Å2 of compound **34**.

The radius of gyration (RoG) is an indicator of molecular compactness and is defined by the distribution of atoms of the molecule with respect to its own axis. An increase in the RoG above the expected value indicates destabilisation of the protein-ligand complex. The mean RoG of BChE and BChE complexed with compounds **34**, **37** and donepezil was found to be 23.066 ± 0.056, 23.146 ± 0.066, 23.133 ± 0.067 and 23.182 ± 0.073 Å, respectively. RoG indicated that the complexes were stable similar to the uninhibited protein. The RoG(s) of the compounds **34**, **37** and donepezil were also found to be stable throughout the simulation with mean values of 4.603 ± 0.115, 4.482 ± 0.205 and 4.311 ± 0.199 Å, respectively (**Figure 4.11**). The sulfonamide group was responsible for prominent hydrogen bonding for compounds **34** and **37**. The hydrogen bond analysis of compound **34** displayed a denser hydrogen bond network than others, with Tyr440 as a major residue. In contrast, the hydrogen bonding of donepezil with the enzyme was the weakest, which could explain its higher IC_{50} value (**Figure 4.12**). The binding free energy obtained from the MM-GBSA is reported in **Table 4.8**.

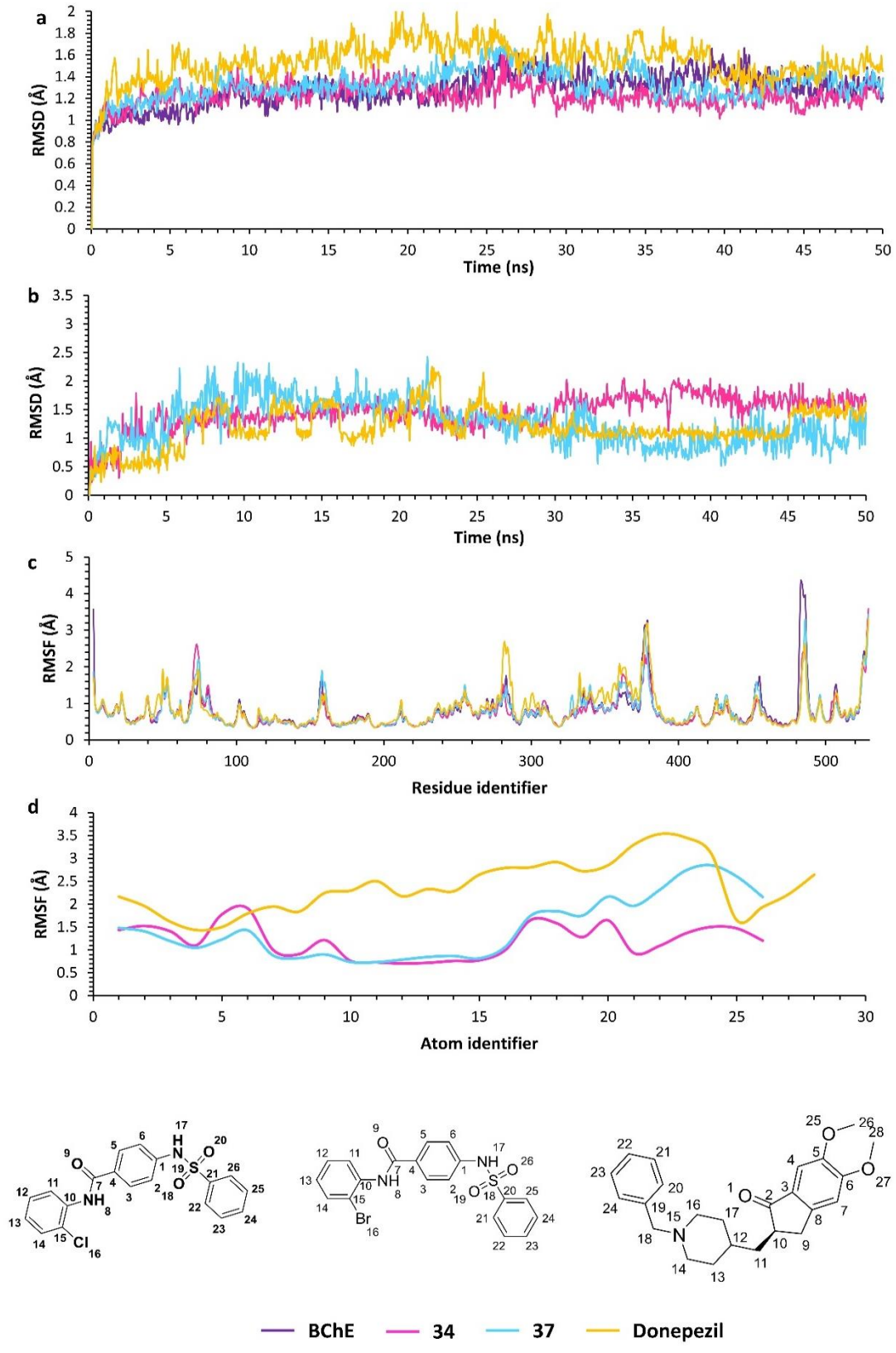

Figure 4.10 RMSD and RMSF analysis of BChE, BChE complexed with compounds **34**, **37** and donepezil: (a) RMSD of protein backbone. (b) RMSD of heavy atoms of ligands. (c) RMSF of protein backbone. (d) RMSF of heavy atoms of ligands

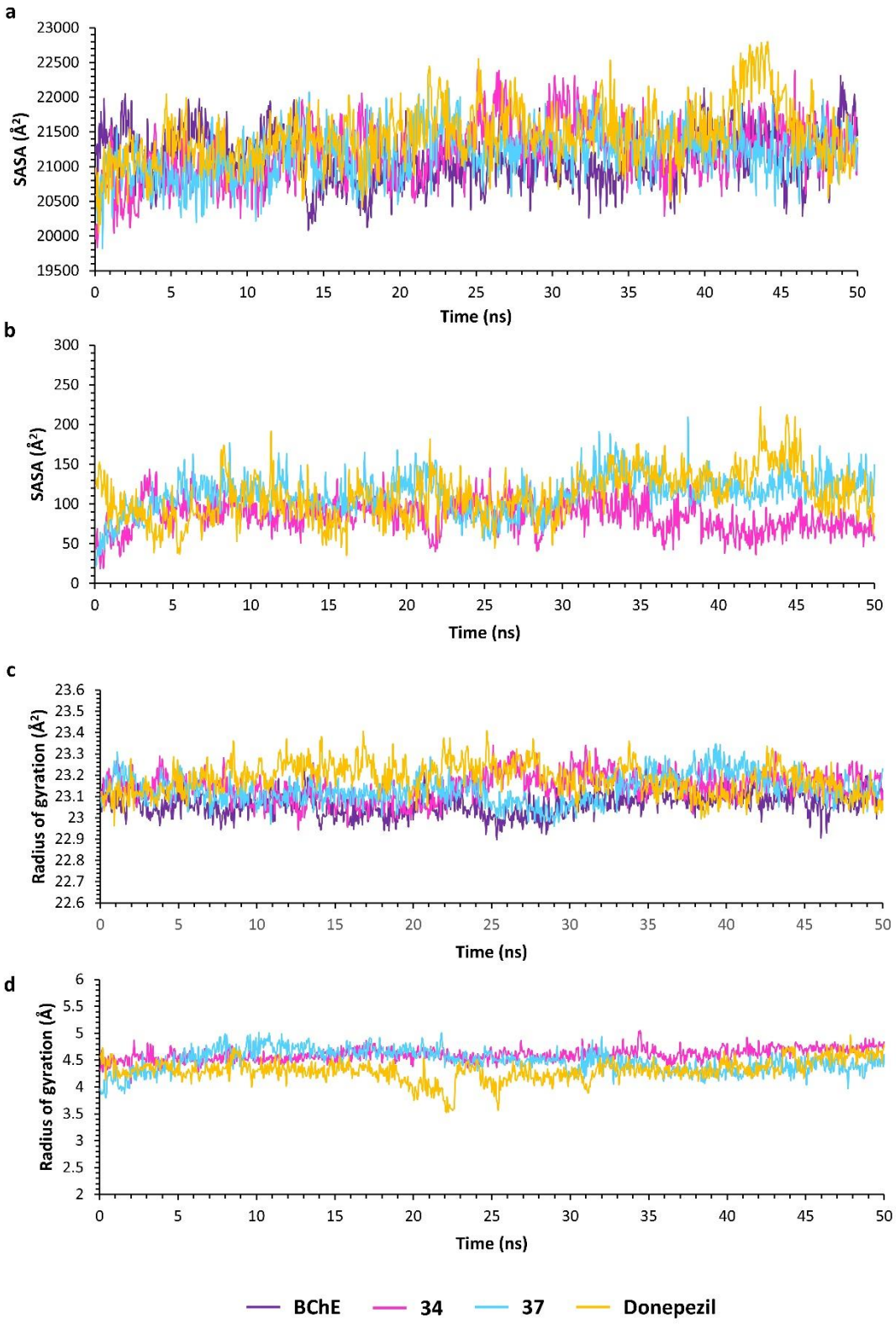

Figure 4.11 SASA and RoG of BChE, complexes of compounds **34**, **37** and donepezil with BChE: (a) SASA of complexes (b) SASA of ligands (c) RoG of complexes (d) RoG of ligands.

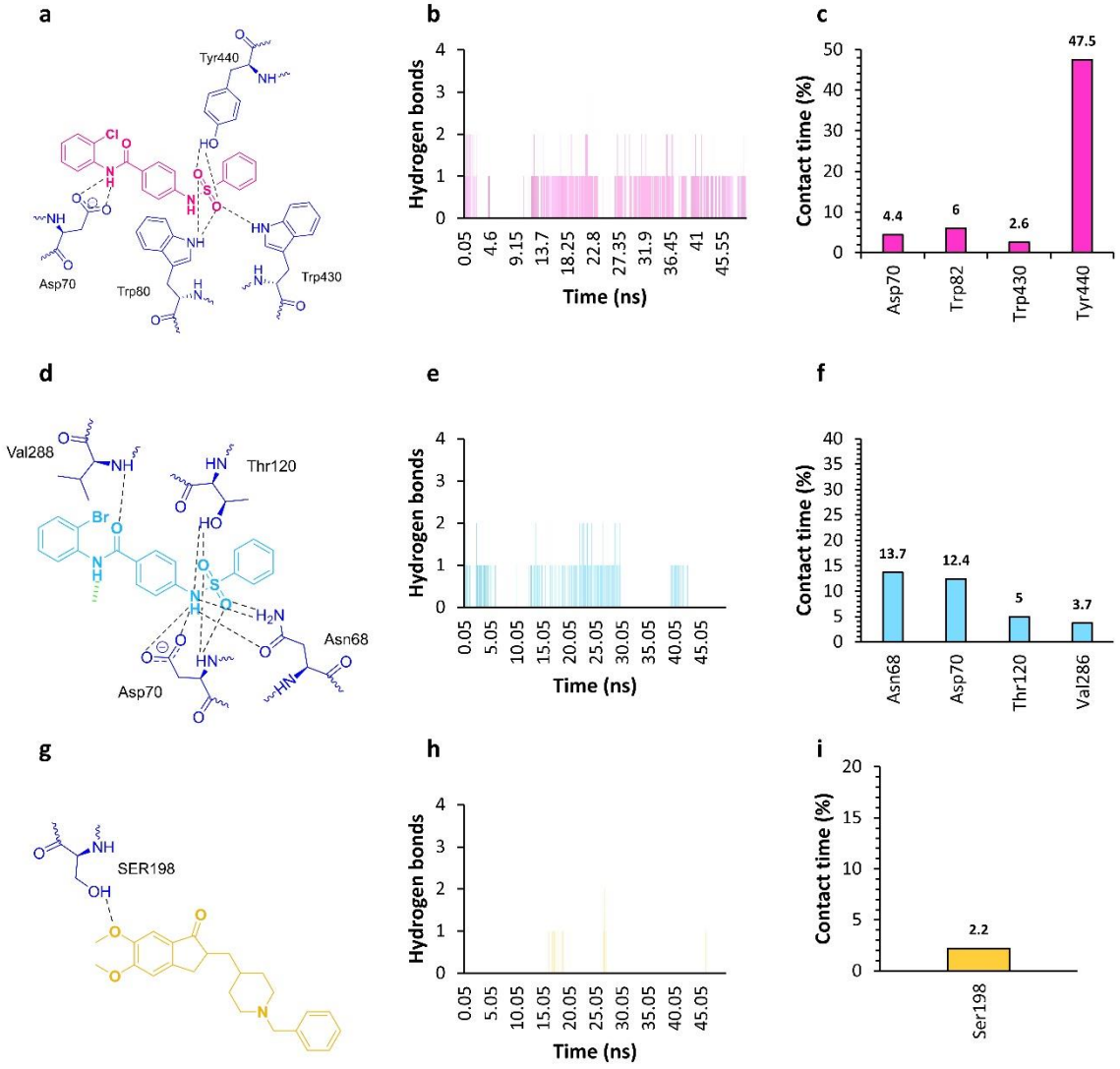

Figure 4.12 Hydrogen boing analysis:(a, d, g) Hydrogen bond interactions of compounds **34, 37** and donepezil with BChE during MD simulation. (b, e, h) Hydrogen bond interactions with respect to simulation time of compounds **34, 37** and donepezil with BChE. (c, f, i) % Contact time of various interacting BChE residues with compounds **34**, **37** and donepezil.

Table 4.7 Energy contributions of protein-ligand complexes obtained from MM-GBSA calculation.

Compound code	ΔE_{vdw}	ΔE_{ele}	ΔG_{GB}	ΔG_{SA}	ΔG_{MMGBSA}
34	-46.013 ± 0.296	-32.566 ± 1.016	43.845 ± 0.916	-6.017 ± 0.0.29	-29.753 ± 0.362
37	-46.306 ± 0.277	-14.213 ± 0.569	40.565 ± 0.5	-5.809 ± 0.034	-25.763 ± 0.382
Donepezil	-44.904 ± 0.332	-6.079 ± 0.405	29.565 ± 0.409	-5.575 ± 0.032	-26.940 ± 0.332

4.3.10. *In vivo* evaluation of compounds

4.3.10.1. Y-maze

4.3.10.1.1. Effect of Scopolamine and various treatments on spontaneous alteration

The effect of SCO treatment resulted in a significant difference in the spontaneous alteration among the groups. The SCO treated group showed a significant reduction in the spontaneous alteration ($P < 0.001$, group: II vs. I). The treatment with donepezil displayed significant improvement in spontaneous alteration ($P < 0.001$, group: III vs. II). The treatment with compound **34** resulted in significant improvement in impaired spontaneous alteration at a dose of 10 mg/Kg ($P < 0.01$, group: V vs II) and 20 mg/Kg ($P < 0.01$, group: VI vs II). Compound **37** also displayed improvement in the spontaneous alteration at 10 mg/Kg ($P < 0.05$, group: VII vs. II) and 20 mg/Kg ($P < 0.01$, group: IX vs. II). There was no significant improvement in spontaneous alteration at a dose of 5 mg/Kg of both the compounds (**Figure 4.13 (a)**).

4.3.10.1.2. Effect of Scopolamine and various treatments on novel arm entries

SCO treatment indicated a significant reduction in the number of novel arm entries as compared to the control group ($P < 0.001$, group: II vs I). The treatment of donepezil displayed a significant improvement in the novel arm entries ($P < 0.001$, group: III vs. II). In case of compound **34**, significant improvement in the number of novel arm entries were observed at doses 10 and 20 mg/Kg ($P < 0.001$, groups: V vs. II and VI vs. II). However, there was no significant improvement in the novel arm entries at a dose of 5 mg/Kg in comparison to SCO, while a considerable difference with donepezil treated group ($P < 0.001$, group: IV vs. III) was observed. On the other hand, compound **37** showed a substantial increase in the number of the novel arm entries at 5 ($P < 0.05$, group: VII vs. II), 10 ($P < 0.001$, group: VIII vs. II) and 20 mg/Kg ($P < 0.001$, group: IX vs. II) (**Figure 4.13 (b)**).

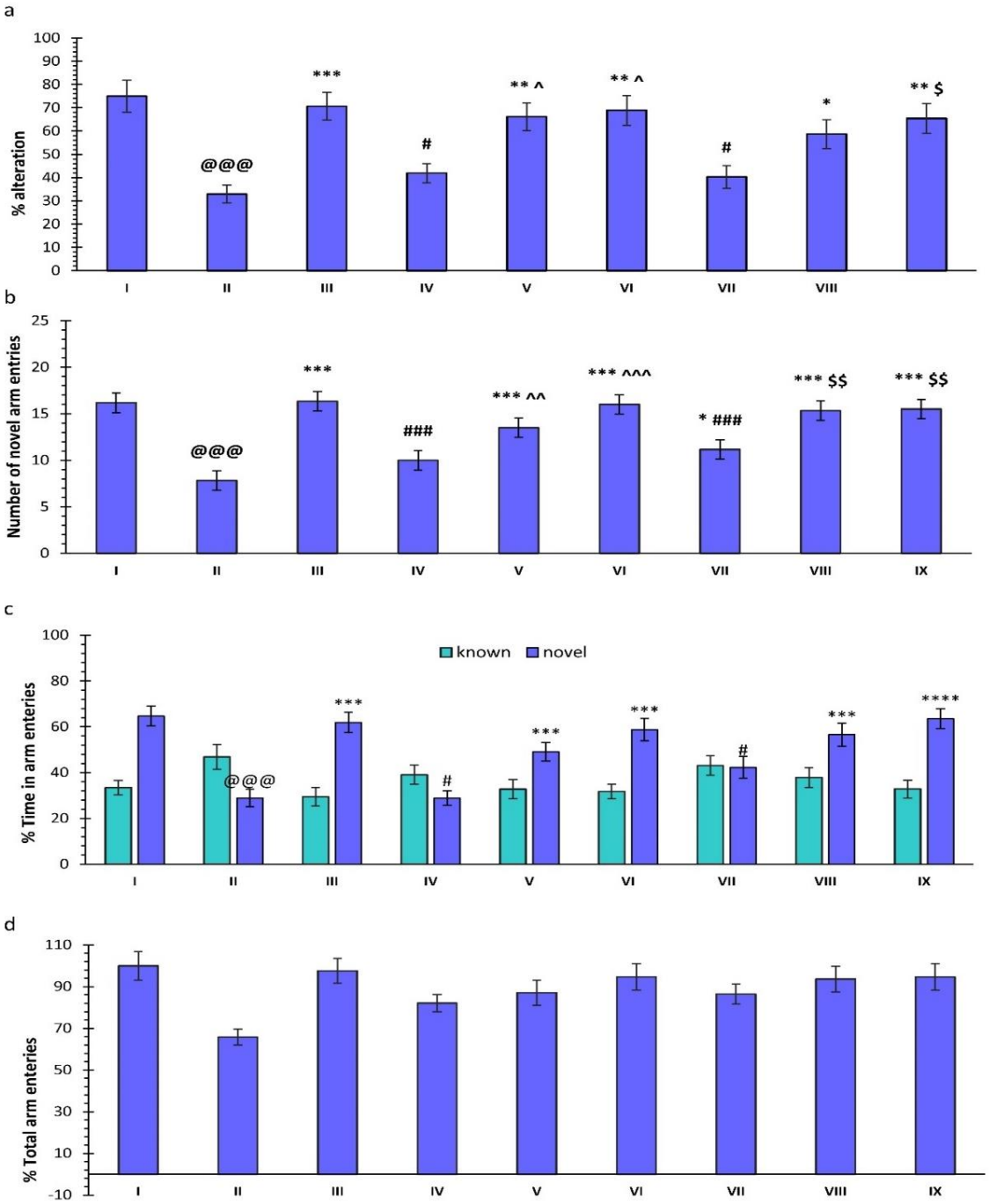

Figure 4.13 Effect of compounds **34**, **37** and donepezil on (a) scopolamine-induced impairment of % spontaneous alteration, (b) novel arm entries, (c) % arm entries and (d) % total arm entries.

Data ara expressed in Mean ± SEM. (N = 6, $^{@@@}$ P < 0.001 compared to control, *** P < 0.001 compared to SCO, ** P < 0.01 compared to SCO, * P < 0.05 compared to SCO, $^{\#}$ P < 0.05 compared to donepezil, $^{\#\#\#}$ P < 0.001 compared to donepezil, $^{\wedge}$ P < 0.05 compared to compound **34**(5 mg/Kg), $^{\wedge\wedge}$ P < 0.01 compared to compound **34**(10 mg/Kg), $^{\wedge\wedge\wedge}$ P < 0.001 compared to compound **34**(20 mg/Kg), $^{\$}$ P < 0.05 compared to compound **37**(5 mg/Kg), $^{\$\$}$ P < 0.01 compared to compound **37**(10 mg/Kg)).

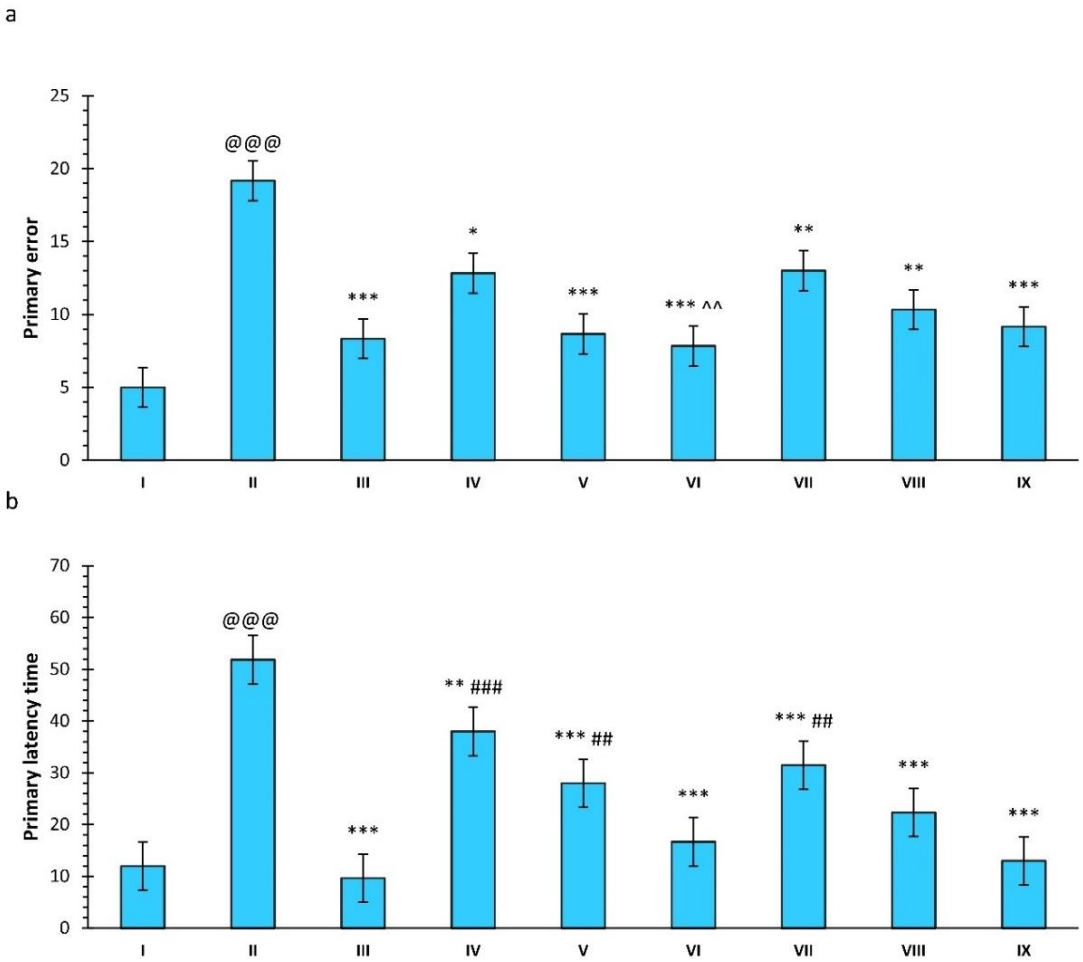

Figure 4.14 Effect of compounds **34**, **37** and donepezil on (a) primary error, (b) primary latency time.

Data are expressed in Mean ± SEM.(N =6, $^{@@@}$ P < 0.001 compared to control, *** P < 0.001 compared to SCO, ** P < 0.01 compared to SCO, * P < 0.05 compared to SCO, $^{###}$ P < 0.001 compared to donepezil, , $^{##}$ P < 0.01 compared to donepezil, $^{#}$ P < 0.05 compared to donepezil, $^{\wedge\wedge\wedge}$ P < 0.001 compared to compound **34**(20 mg/Kg), $^{\wedge\wedge}$ P < 0.01 compared to compound **34**(10 mg/Kg), $^{\wedge}$ P < 0.05 compared to compound **34**(5 mg/Kg), $^{\$\$\$}$ P < 0.001 compared to compound **37**(20 mg/Kg), $^{\$\$}$ P < 0.01 compared to compound **37**(10 mg/Kg), $^{\$}$ P < 0.05 compared to compound **37**(5 mg/Kg))

4.3.10.1.3. Effect of Scopolamine and various treatments on novel and known arm entries

SCO treatment did not result in overall significant change in the known arm entry among the groups. However, there was a slight increase in the time spent in the known arm in the SCO treated group. Further, there was a significant decrease in time spent (% time) in the novel arm in SCO treated group (P < 0.001, group: II vs. I) as compared to control. The treatment with donepezil also caused a significant increase in % time spent in the novel arm (P < 0.001, group: III vs. II). Compound **34**, at the dose of 5 mg/Kg, did not show significant improvement in % time spent in the novel arm in comparison to SCO treated group. But the higher doses caused a significant improvement in the time (P <

0.001, groups: V vs. II and VI vs. II). Compound **37** displayed a significant improvement in % time spent in the novel arm at doses 10 and 20 mg/Kg ($P < 0.001$, groups: VIII vs. II and IX vs. II) compared to SCO. On the other hand, the % time spent in the novel arm was improved at 5 mg/Kg, but no significant difference was observed as compared to the SCO group (**Figure 4.13 (c)**).

4.3.10.1.4. Effect of Scopolamine and various treatments on total arm entries

There was no significant difference in total % arm entries among the various groups (**Figure 4.13 (d)**).

4.3.10.2. Barnes maze

4.3.10.2.1. Effect of scopolamine and various treatments on primary errors

SCO administration to the rats resulted in a significant increase in the primary error ($P < 0.001$, group II vs. I). On the other hand, significant improvement was observed in case of donepezil treatment, as compared to the SCO group ($P < 0.001$, group: III vs. II). The treatment with compound **34** showed significant decrease in primary error at 5 mg/Kg ($P < 0.05$, group: IV vs. II) and improvement in error at doses 10 ($P < 0.001$ vs. SCO) and 20 ($P < 0.001$ vs. SCO) mg/Kg. Compound **37**, produced significant improvement in all the treatment groups as compared to the control (**Figure 4.14(a)**).

4.3.10.2.2. Effect of scopolamine and various treatments on primary latency time

SCO treatment group displayed an increase in the primary latency ($P < 0.001$, group: II vs. I) in comparison to the control. A significant reduction in primary latency was observed in the case of both compounds **34** and **37**. The dose of 20 mg/Kg showed maximum reduction in the primary latency ($P < 0.001$, group: VI vs. II and IX vs. II) for both compounds as compared to SCO (**Figure 4.14(b)**).

4.3.10.3. Neurochemical analysis

4.3.10.3.1. Effect of scopolamine and various treatments on total cholinesterase activity

The total ChE activity of hippocampus and PFC, with ATCI as substrate, was found to be significantly increased in SCO treated group when compared with the control ($P < 0.001$, group: II vs. I). Donepezil displayed a significant decrease in activity ($P < 0.001$, group: III vs. II) but, no significant decrease was observed in case of the other treatment groups as compared to SCO group. On the other hand, there was a significant inhibition in total ChE activity of PFC with ATCI as a substrate for compounds **34** and **37** at a dose of 20 mg/Kg ($P < 0.05$, groups: VI vs. II and IX vs. II). The treatment with donepezil also displayed a significant reduction in ChE activity of PFC ($P < 0.001$, group: III vs. II). The total ChE activity, with BTCI as a substrate, produced exciting results. The total ChE activity of hippocampus and PFC, with BTCI as substrate, was also increased significantly in SCO treated group in comparison to the control ($P < 0.001$, group: II vs. I). A significant reduction in enzyme activity was observed at doses 10 mg/Kg ($P < 0.05$, groups: V vs. II for **34** and VIII vs. II for **37**) and 20 mg/Kg ($P < 0.001$, group: VI vs II for **34** and $P < 0.01$, group: IX vs. II for **37**) in the hippocampus. Similarly, significant inhibition was observed in ChE activity in PFC for compounds **34** and **37** at a dose of 10 ($P < 0.05$, groups: V vs. II for **34** and VIII vs. II for **37**) and 20 mg/Kg ($P < 0.001$, group: VI vs. II and $P < 0.01$, group: IX vs. II). Interestingly, no significant cholinesterase inhibition for donepezil treatment was found in both hippocampus and PFC with BTCI as substrate (**Figure 4.15**).

4.3.10.3.2. Effect of scopolamine and various treatments on CAT activity

The SCO treatment also caused a reduction in the CAT activity with respect to the control group ($P < 0.001$, group: II vs. I). However, treatment with donepezil and the selected compounds displayed significantly higher CAT activity than SCO treated group in both

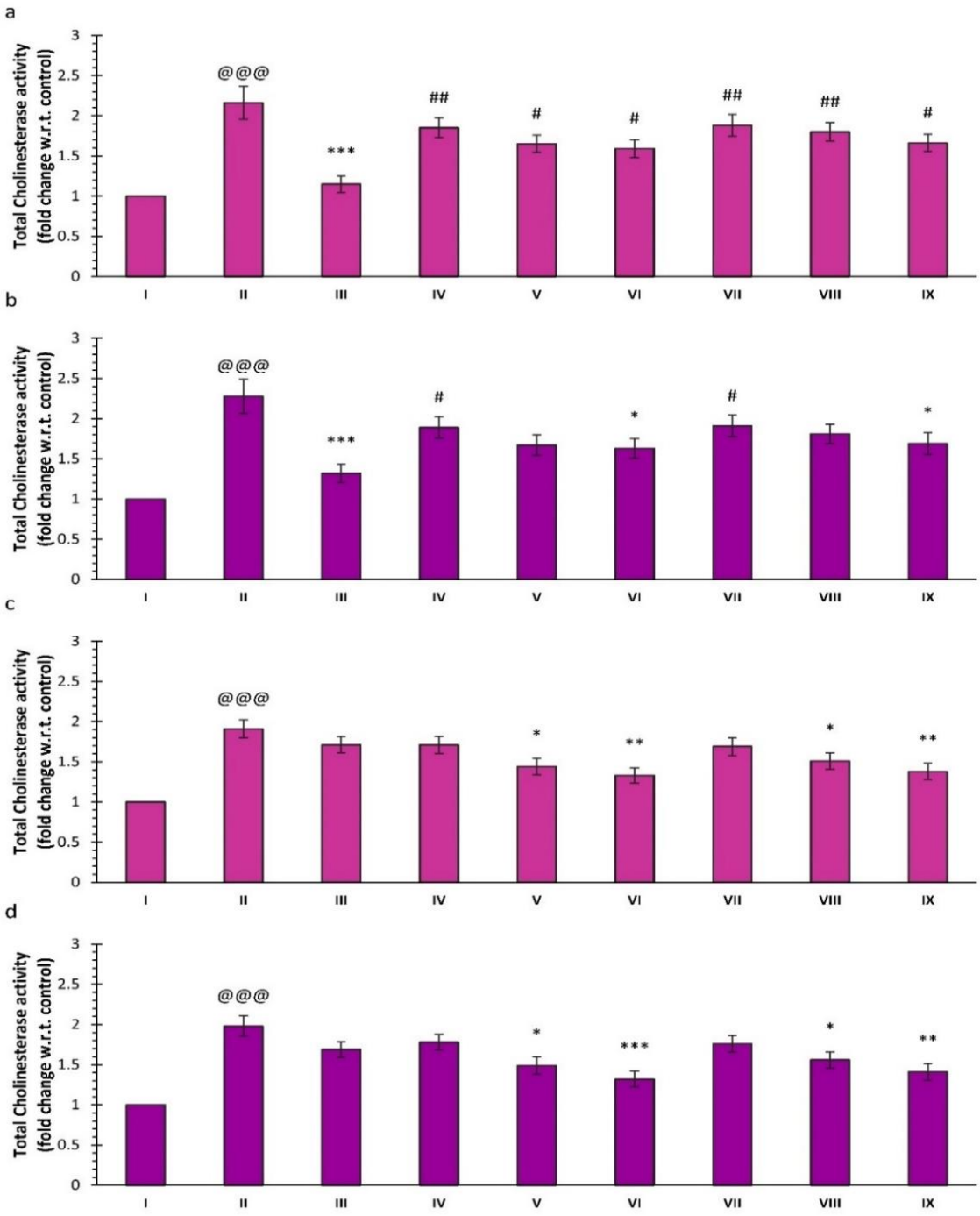

Figure 4.15 Effect of compounds **34**, **37** and donepezil on total cholinesterase activity with ATCI as substrate in (a) hippocampus, (b) PFC and with BTIC as substrate in (c) hippocampus, (d) PFC.

Data are expressed in Mean ± SEM. (N = 6, $^{@@@}$ P < 0.001 compared to control, *** P < 0.001 compared to SCO, ** P < 0.01 compared to SCO, * P < 0.05 compared to SCO, $^{###}$ P < 0.001 compared to donepezil, , $^{##}$ P < 0.01 compared to donepezil, $^{#}$ P < 0.05 compared to donepezil, $^{\wedge\wedge\wedge}$ P < 0.001 compared to compound **34**(20 mg/Kg), $^{\wedge\wedge}$ P < 0.01 compared to compound **34**(10 mg/Kg), $^{\wedge}$ P < 0.05 compared to compound **34**(5 mg/Kg), $^{\$\$\$}$ P < 0.001 compared to compound **37**(20 mg/Kg), $^{\$\$}$ P < 0.01 compared to compound **37**(10 mg/Kg), $^{\$}$ P < 0.05 compared to compound **37**(5 mg/Kg))

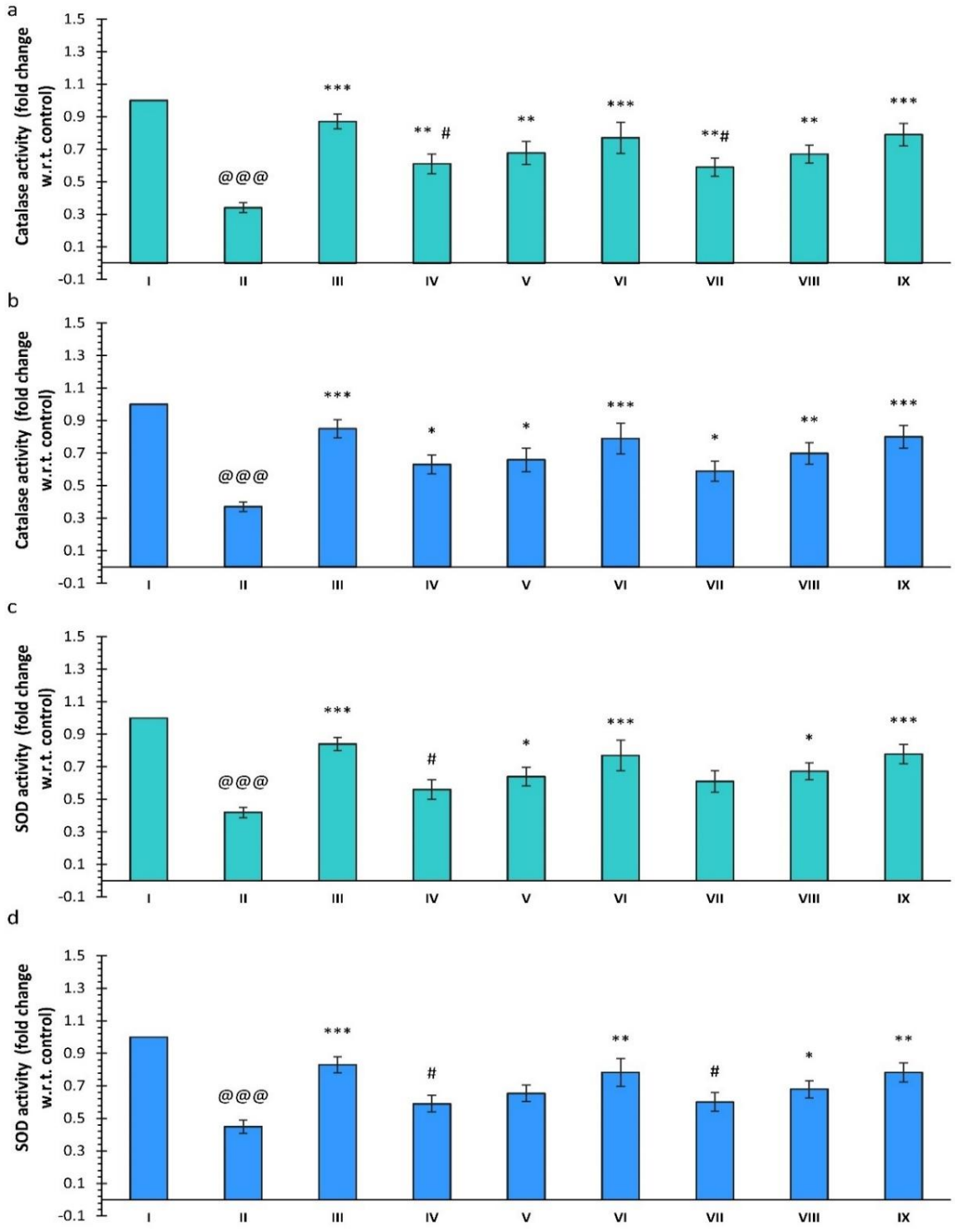

Figure 4.16 Effect of compounds **34**, **37** and donepezil on CAT activity in (a) hippocampus, (b) PFC and SOD activity in (c) hippocampus, (d) PFC.

Data are expressed in Mean ± SEM. (N = 6, $^{@@@}$ P < 0.001 compared to control, *** P < 0.001 compared to SCO, ** P < 0.01 compared to SCO, * P < 0.05 compared to SCO, $^{###}$ P < 0.001 compared to donepezil, , $^{##}$ P < 0.01 compared to donepezil, $^{#}$ P < 0.05 compared to donepezil, $^{\wedge\wedge\wedge}$ P < 0.001 compared to compound **34**(20 mg/Kg), $^{\wedge\wedge}$ P < 0.01 compared to compound **34**(10 mg/Kg), $^{\wedge}$ P < 0.05 compared to compound **34**(5 mg/Kg), $^{\$\$\$}$ P < 0.001 compared to compound **37**(20 mg/Kg), $^{\$\$}$ P < 0.01 compared to compound **37**(10 mg/Kg), $^{\$}$ P < 0.05 compared to compound **37**(5 mg/Kg))

hippocampus and PFC. Both the compounds showed maximum hippocampal CAT activity at a dose of 20 mg/Kg, with no significant difference observed when compared with donepezil. Further, CAT activity of PFC was also found to be significantly higher at a dose of 20 mg/Kg ($P < 0.001$, group: IX vs. II) as compared to the disease group but no significant difference was observed when compared to the donepezil (**Figure 4.16**).

4.3.10.3.3. Effect of scopolamine and various treatments on SOD activity

SCO treatment also caused a significant reduction in the SOD activity with respect to the control group ($P < 0.001$, group: II vs. I) in both hippocampus and PFC. In contrast, the treatment with donepezil showed significantly higher SOD activity in both regions ($P < 0.001$, group: III vs. II). The treatment with 20 mg/Kg dose of compounds **34** and **37** showed significantly higher SOD activity in the hippocampus ($P < 0.001$, groups: VI vs. II and IX vs. II). The activity of SOD was significantly higher at a dose of 20 mg/Kg for compound **37** in PFC ($P < 0.01$, group: IX vs. II) (**Figure 4.16**).

4.3.10.4. Biochemical analysis

The biochemical analysis of SGPT and SGOT enzymes did not indicate any significant difference between the control and the treatments. Similarly, no significant difference was observed among the control and the treatment groups for serum creatinine and urea levels (**Figure 4.17**).

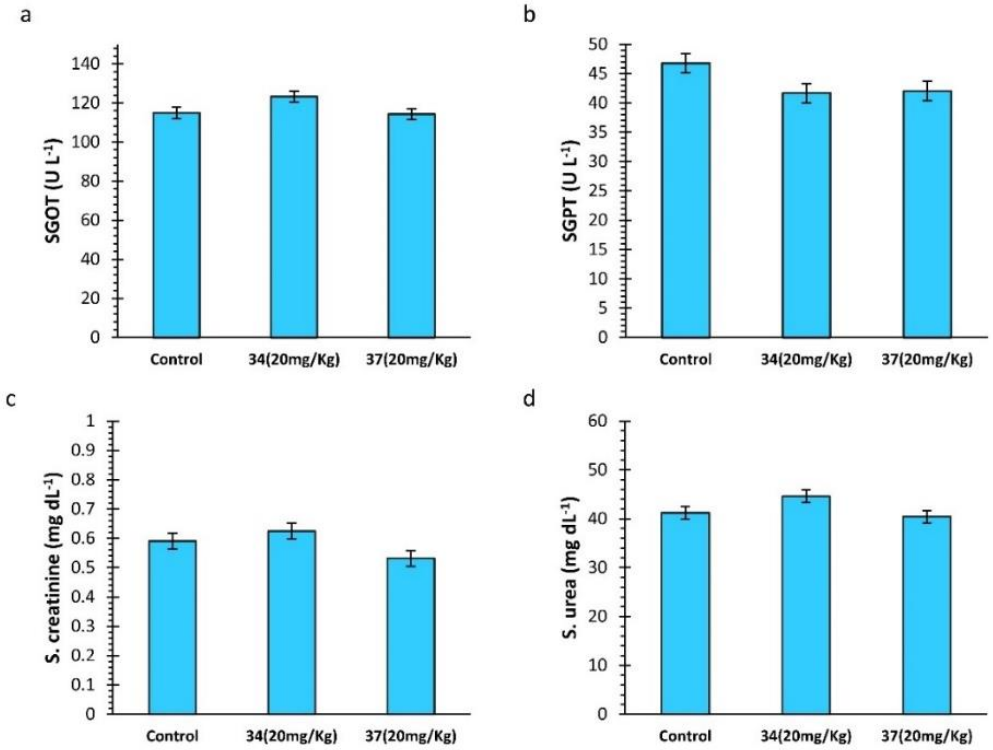

Figure 4.17 Effect of compounds **34** and **37** on (a) SGOT, (b) SGPT, (c) Serum creatinine and (d) Serum urea levels.
Data are expressed in Mean ± SEM.